Nanoscale Research Letters

NANO REVIEW

Open Access

Status and Prospects of ZnO-Based Resistive Switching Memory Devices

Firman Mangasa Simanjuntak[1], Debashis Panda[2], Kung-Hwa Wei[1] and Tseung-Yuen Tseng[3*]

Abstract

In the advancement of the semiconductor device technology, ZnO could be a prospective alternative than the other metal oxides for its versatility and huge applications in different aspects. In this review, a thorough overview on ZnO for the application of resistive switching memory (RRAM) devices has been conducted. Various efforts that have been made to investigate and modulate the switching characteristics of ZnO-based switching memory devices are discussed. The use of ZnO layer in different structure, the different types of filament formation, and the different types of switching including complementary switching are reported. By considering the huge interest of transparent devices, this review gives the concrete overview of the present status and prospects of transparent RRAM devices based on ZnO. ZnO-based RRAM can be used for flexible memory devices, which is also covered here. Another challenge in ZnO-based RRAM is that the realization of ultra-thin and low power devices. Nevertheless, ZnO not only offers decent memory properties but also has a unique potential to be used as multifunctional nonvolatile memory devices. The impact of electrode materials, metal doping, stack structures, transparency, and flexibility on resistive switching properties and switching parameters of ZnO-based resistive switching memory devices are briefly compared. This review also covers the different nanostructured-based emerging resistive switching memory devices for low power scalable devices. It may give a valuable insight on developing ZnO-based RRAM and also should encourage researchers to overcome the challenges.

Keywords: Resistive switching, Resistive memory, RRAM, Memristor, ZnO, Nonvolatile memory

Review

Introduction

Semiconductor memory is an indispensable component and backbone of all modern electronic devices. All recognizable computing platforms ranging from hand-held devices to large super-computer storage systems are used for storing data, either temporarily or permanently, as per their requirement [1]. Based on storing data volatility, memories are basically classified into two categories, (i) volatile memory and (ii) nonvolatile memory. In a volatile memory, the stored data is lost immediately after the power is turned off whereas nonvolatile memory (NVM) is capable to retain the stored data for a long time even after the power is off. Demands on NVMs are increasing extensively, due to the huge popularity of consumer electronics and portable gadgets, such as smart phone, memory card, and USB storage devices, where NVM is one of the basic component [2–5].

Over the last few decades, a variety of NVM devices such as flash memory, resistive random access memory (RRAM), phase change memory (PCM), ferroelectric memory (FeRAM), and magnetic random access memory (MRAM) have emerged, though each has some technical limits, such as scalability, retention, switching power, and reliability aspects [2, 5–33]. Among them, resistive switching memory devices are expected to be one of the promising candidates for future nanoscale memories [34–46].

RRAM Technology

In 1971 [47, 48], memristor (memory-resistor), later also called as resistive switching memory [31, 32], is firstly introduced and theorized as the fourth classical circuit elements by Chua. The element was realized in the form of active circuit which then behaves like a nonlinear resistor with memory [47]. A few years before the

* Correspondence: tseng@cc.nctu.edu.tw
[3]Department of Electronics Engineering and Institute of Electronics, National Chiao Tung University, Hsinchu 30010, Taiwan
Full list of author information is available at the end of the article

Springer Open

© 2016 The Author(s). **Open Access** This article is distributed under the terms of the Creative Commons Attribution 4.0 International License (http://creativecommons.org/licenses/by/4.0/), which permits unrestricted use, distribution, and reproduction in any medium, provided you give appropriate credit to the original author(s) and the source, provide a link to the Creative Commons license, and indicate if changes were made.

introduction of the new element, nonlinear resistance changes had been observed in various metal oxides [49]. Gibbons and Beadle, in 1964 [50], proposed the existence of conducting filament (CF) to control the resistance changes in Ag/NiO/Ni device. However, the origin of such conduction is not explored until Simmons and Verderber in 1967 [51] suggested that the conduction of reversible switching in Au/SiO/Al device was originated from the conduction electrons travel by tunnelling between sites provided by Au ions injected from Au electrode. These findings may lead to the development of RRAM applications. Nowadays, the role of CF is acknowledged to be as a "circuit breaker" that determine the principle of the switching itself [37]. Much efforts has been conducted to modulate its shape, size, and number and to understand the mechanism that define the switching behavior [52–56].

Advantages of ZnO for RRAM Applications

Resistive random access memory have been developed in various structures, such as sandwich [52–56], planar [57, 58], laterally bridge [59], single nanorod/nanowire [60–75], nanobelt [76], and nanoisland [77, 78]. Nevertheless, the basic RRAM structure should consist of two opposite electrodes and a storage material, as depicted in Fig. 1. Organic [79], inorganic [44,] or hybrid [80] insulating materials can be used as a storage material for the RRAM applications. Among them, inorganic materials, metal oxides, gained huge interest for the use as storage materials due to its wide range of electrical properties [39]. Among numerous metal oxides, ZnO has advantageous properties such as low cost, wide and direct band gap of ~3.3 eV, low synthetic temperature, controllable electrical behavior, chemically stable, electrochemical activity, biocompatible, and environmental friendly [81, 82]. ZnO can be grown with wide variety of morphologies [81, 82], such as nanowires, nanorods, terapods, nanoribbons/belts, hierarchical, bridge-/nail-like, tubular, nanosheets, nanopropeller, nanohelixes, and nanorings which may open the opportunity to fabricate various one-dimensional RRAM structures. Due to its exceptional advantages and various morphologies, ZnO has been also considered as a promising candidate in broad practical applications [81, 82], such as piezoelectric transducers, bio sensors, chemical and gas sensors, optical waveguides, photo detector, photovoltaics, surface acoustic wave devices, varistors, transparent conductive oxides, spin functional devices, and UV-light emitters. These wide applications may open the possibility to design nonvolatile resistive switching memories with multifunctional features which will be discussed later.

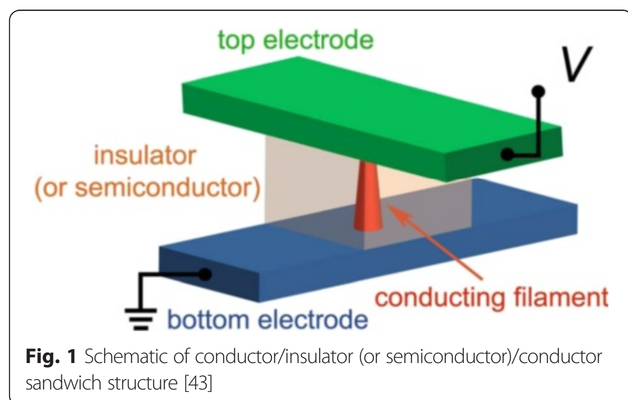

Fig. 1 Schematic of conductor/insulator (or semiconductor)/conductor sandwich structure [43]

Switching Mechanism in Oxide-Based RRAM

Computer data are read in the sense of binary code "1" and "0." Accordingly, data stored in resistive memory devices are differentiated by its resistance state, so called "low resistance state (LRS)" or "ON" and "high resistance state (HRS)" or "OFF" states. These states can be switched reversely using electric stimulus. The switching process from HRS to LRS and LRS to HRS are named as set and reset, respectively. Current compliance (I_{comp}) is normally applied to prevent hard breakdown during set. Resistive memory operates under either unipolar or bipolar operation mode. In unipolar mode, depicted in Fig. 2a, set and reset processes occur in the same bias polarity. Conversely, in bipolar mode, opposite bias polarities are required to set and reset a device, as depicted in Fig. 2b. These modes are dependent on device structure [44, 45, 83] and electrical operation setup [31, 84]. However, coexistence of bipolar and unipolar in the same device was also reported [85–88]. Nevertheless, general understanding on unipolar and bipolar modes can be concluded upon the factors that trigger the reset process. In unipolar, Joule heating is the main driving force to rupture a CF during reset, whereas in bipolar, dissolution of CF is due to the migrating charged species, yet Joule heating still contributes to accelerate the migration [42, 45].

Generally, based on the chemical effects involved in the switching process, RRAM can be classified as electrochemical metallization memory (ECM) and valence change memory (VCM) [44]. ECM, also known as conductive bridge CBRAM, relies on an electrochemically active metal electrode [42] such as Ag, Cu, or Ni, to form metal cation-based CF. On the other hand, CF in VCM cell is composed of oxygen vacancies defects, instead of metal atoms, due to anion migration within the storage material itself [31]. This CF size in the range of 20–30 nm strongly depends upon the amount of current flowed during forming and set [45, 89].

In filamentary model, the set current mainly flows through the CF [46]. The filament size is considerably smaller than electrode area that leads to localized conduction effect; thus, LRS is independent on electrode size [46, 86, 90]. Apart from the filamentary model,

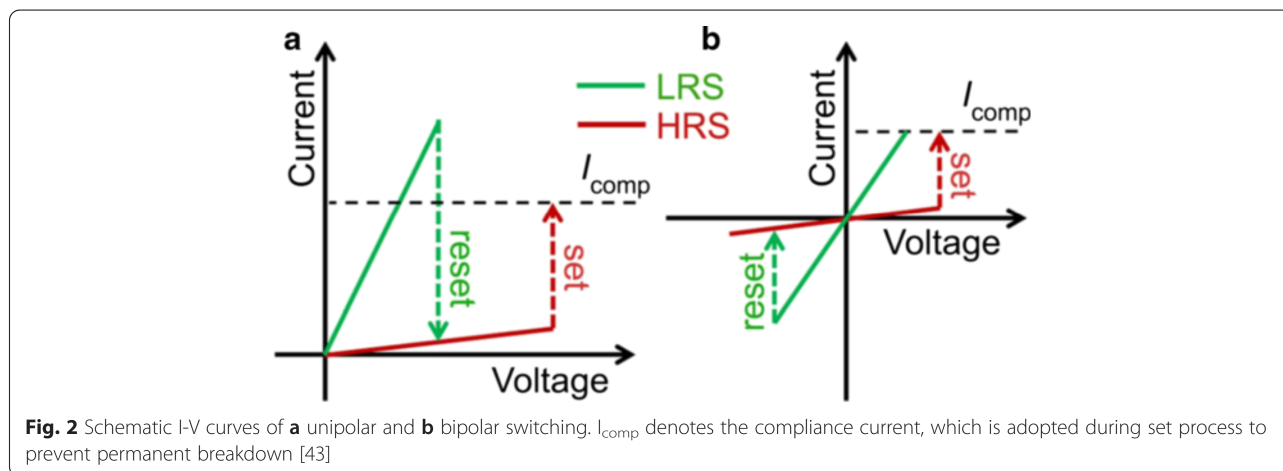

Fig. 2 Schematic I-V curves of **a** unipolar and **b** bipolar switching. I_{comp} denotes the compliance current, which is adopted during set process to prevent permanent breakdown [43]

homogeneous interface-type model was also proposed in switching mechanism of VCM cell [43]. In homogeneous interface-type model, both set and reset current flow homogenously over the entire electrode area; thus, LRS and HRS are proportional to the electrode area [44]. The conduction is determined by the field-induced change of the Schottky barrier height at the electrode/storage material interface [42, 44]. Interface-type device can be designed by sandwiching the storage material with Ohmic and Schottky contacts [43, 91] or modulating oxide/oxide interface in multilayer device [83].

The filamentary switching can be transformed into homogeneous switching [84] by modulating the measurement parameters. Figure 3 shows the transformation of filamentary into homogeneous switching in a typical Pt/ZnO/Pt device [84]. The transformation was conducted by introducing a reverse sweep bias with high I_{comp} after initiating unipolar switch leading to the formation of oxygen-defective region near the bottom electrode, as depicted in the inset of Fig. 3b [84]. This region can also be modulated simply by applying various I_{comp} or reset voltage (V_{reset}); hence, multilevel characteristic was observed. Multilevel characteristics having more than two resistance states can be an effective way to increase storage density besides device size scaling [42, 92]. Homogeneous switching dependent on device area guarantees a sufficient current to maintain reliable operation, whereas filamentary may suffer from switching instability in a scaled down device [84]. Nevertheless, filamentary exhibits superior retention due to the aligned conducting channel, since in homogenous switching, oxygen vacancies from interface tend to diffuse back to the bulk through the grain boundaries leading to poor retention performance [91].

Origin of Conducting Filament CF is formed in ECM cell when a positive bias applied on an active electrode that leads to an anodic dissolution at anode/storage material interface, resulting in metal cations diffusing toward the opposite electrode [93]. The cation transfer and mobility are controlled by electron dose, Joule heating, and structural quality of the storage material [93, 94]. Mobility also controls the reduction process occurring either before or after the cations reach the opposite electrode

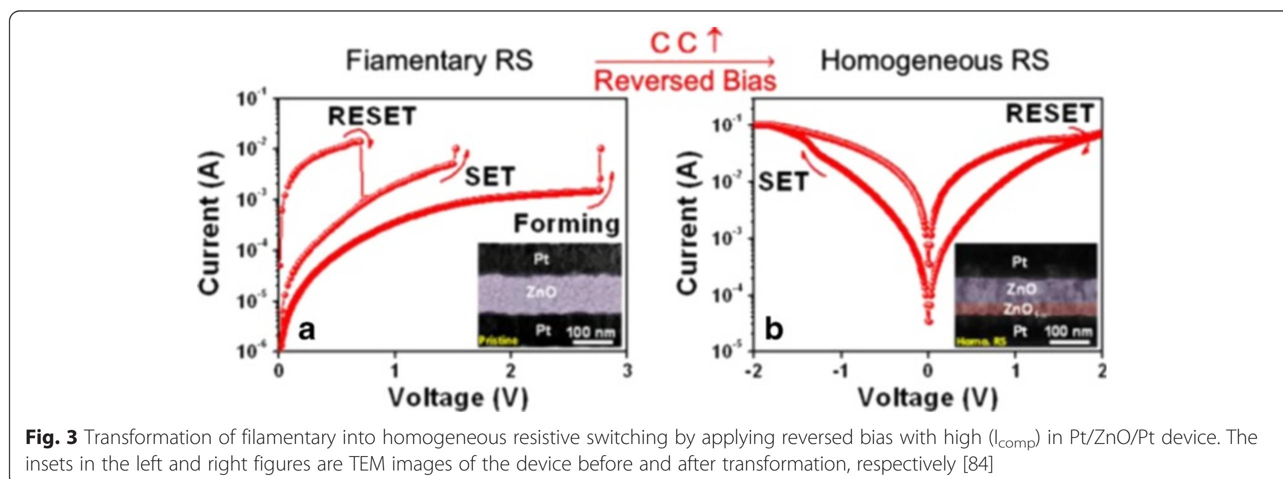

Fig. 3 Transformation of filamentary into homogeneous resistive switching by applying reversed bias with high (I_{comp}) in Pt/ZnO/Pt device. The insets in the left and right figures are TEM images of the device before and after transformation, respectively [84]

[43, 93]. These cations then reduce in the form of tiny metal clusters that grow from anode to cathode or vice versa depending on the mobility [43, 93, 95].

Thus, the construction of these tiny metal clusters across the storage material leads to the formation of a conducting metal bridge (filament) that behaves as an electron conduction channel between the electrodes [93, 94]. During reset or rupture process, Joule heating is mostly dominated at the narrowest part of the filament, which is most known as the filament dissolution process [43, 95].

Unlike ECM cell that relies on metal cation migration from active anode, the formation of CF in VCM cell is due to the migration of oxygen ions and oxygen vacancy defects that generated within the storage material itself. When a positive bias is applied on anion-active anode, oxygen ions move toward anode; reversely, oxygen vacancies move toward cathode [43]. The percolation of oxygen vacancies across the storage material acts as an acceptor for electron carriers [43]. Yet, the physical mechanism of CF formation in VCM is a good area of research.

Kwon et al. [96] suggest that CF in TiO_2 system is an ordered structure, Magnéli phase, that is spontaneously formed under electric field and thermal effect. Magnéli phase possess high electron conductivity near room temperature [97]. However, Kwon et al. [98] argue that the formed Magnéli phase is just as a virtual electrode while set and reset processes are the rejuvenation and dissolution of Wadsley defects, respectively. Wadsley defect can be considered as a missing plane of oxygen atoms in TiO_2 rutile structure [98]. Similarly, Yoon et. al. [99, 100] suggest that a localized TiO_{2-x} layer may act as an active switching region where as rejuvenation and dissolution of Magnéli phase as a switching filament may be insignificant. Nevertheless, formation of a certain conducting phase, like a Magnéli phase in TiO_2, may not be possible in ZnO since it has no stable suboxide phase [101]. Therefore, other mechanisms on the formation of CF could be dominant.

Recent theoretical studies [102, 103] on the formation of CF in ZnO VCM cell suggest that the generated oxygen vacancies moves toward cathode and transform their 2+ charges to neutral thus weaken the Schottky barrier at ZnO/Pt interface, meanwhile the Zn^{2+} is reduced to O-deficient Zn ions ($Zn^{(2-n)+}$) around the respective region. The chemical reaction for these processes can be expressed as [102];

$$O_o^x \rightarrow V_O^{oo} + 1/2O_2 + 2e^- \quad (1)$$

$$V_O^{oo} + 2e^- \rightarrow V_o^x \quad (2)$$

$$Zn^{2+} + ne^- \rightarrow Zn^{(2-n)+} \quad (3)$$

where O_o^x, V_O^{oo}, O_2, e^-, V_o^x, Zn^{2+}, and $Zn^{(2-n)+}$ are a neutral charge of oxygen ion in O site, a doubly positive charge of O vacancy, oxygen gas, a singly negative charge of an electron, a neutral charge of oxygen vacancy, a doubly positive charge of zinc ions, and a reduced positive charge of zinc ions, respectively. Equations 1, 2, and 3 are chemical reaction for the generation of oxygen vacancies, transformation of oxygen vacancies to neutral state, and reduction of zinc metal ions, respectively.

The aligned neutral oxygen vacancy (neutral oxygen vacancy filament), therefore, leads to formation of high conductive $Zn^{(2-n)+}$ filament [102]. Thus, the electrons prefer to conduct trough this metallic filament due to the lower chemical valence state [102, 103]. Conversely, the transformation of oxygen vacancies charge from 2+ to neutral by opposite voltage polarity (bipolar) or Joule heating (unipolar) will lead to oxygen vacancies diffuse from their configuration to other sites, in other words, disruption of filament made by oxygen vacancy [102].

Chen et al. [69, 89] directly observed CF in ZnO cell by utilizing in situ TEM (transmission electron microscope) technique. It was observed that once the oxygen vacancies reach a certain critical density, a newly generated ordered crystalline phase is formed. Figure 4 shows the reset process and structure identification of a CF in Pt/ZnO/Pt cell [89]. It was found that the CF region was identified as a Zn-dominated ZnO_{1-x} metallic phase [89], confirming the formation of zinc metallic filament [102, 103]. This metallic phase can be ruptured when the oxygen ions migrate to this metallic phase region and convert the Zn-dominated ZnO_{1-x} phase back to ZnO phase [69, 89]. Consequently, this evidence shows that the oxygen ion migration plays a critical role in the formation and disruption of a CF.

Despite various advance imaging techniques that have been employed to understand the nature of CF in both metal oxide-based ECM and VCM cell such as scanning transmission x-ray microscope (STXM) [104–106], TEM [69, 89, 93, 94, 96, 98, 107, 108], and C-AFM (conductive-atomic force microscope) [56, 68, 77, 78, 109–114], the relationship between retention behavior and evolution of CF is still less discussed.

Effect of Electrodes in ZnO-Based RRAM Devices

ZnO is generally n-type high-bandgap semiconducting materials. Although the origin of its electron conductivity is still debatable, Zni (zinc interstitial) and Vo (oxygen vacancy) defects are considered to be responsible for the low resistance [115, 116]. Abundant amount of these defects may result in insufficient switching properties. Therefore, several attempts have been reported to improve ZnO as a switching layer, such as stacked with various metal electrodes [117–128], controlled its growth deposition [52, 129–133], post-thermal treated [134, 135], doped with various elements [56, 85–87, 90,

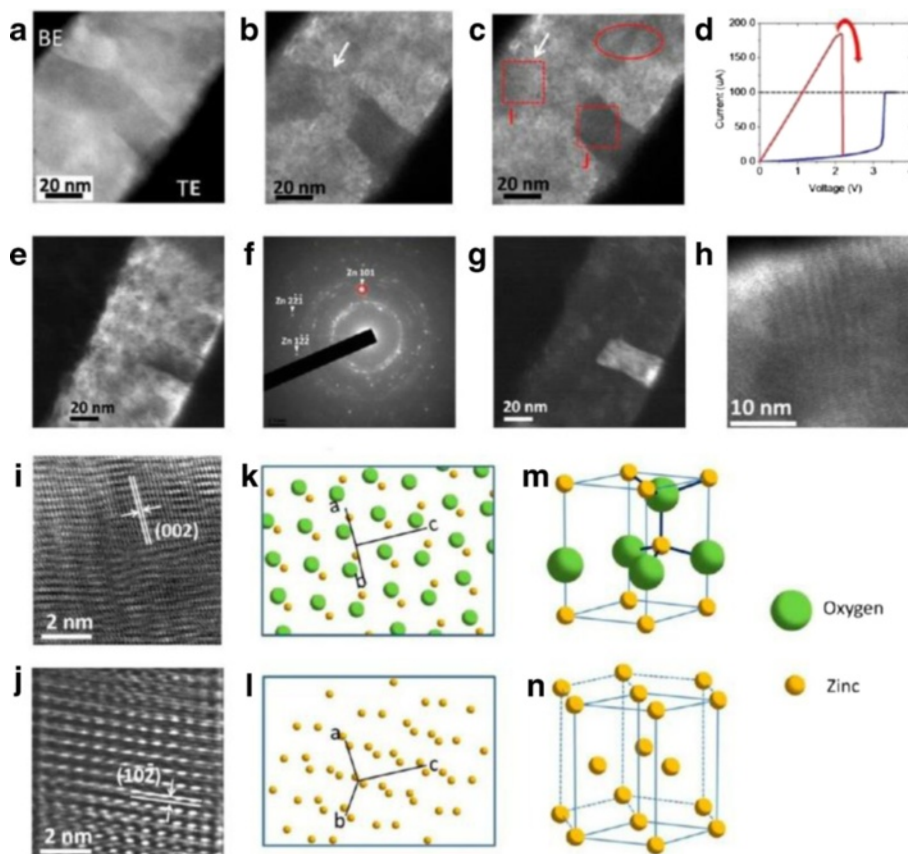

Fig. 4 In situ TEM images of the reset process using the unipolar resistive switching method. **a** The start of recording; **b** intermediate state; **c** final state of the ruptured filament after the reset process. **d** The corresponding I-V curve in *red*; the *blue line* corresponds to the forming process as a comparison. **e** The other conductive filament in the same in situ specimen, indicating that the switching behavior is caused by multi-filament formation and rupture. **f** The selected area diffraction pattern of the conductive filament in Fig. 2e. The Zn (101) diffraction spot is marked with the *red circle*. **g** The corresponding dark-field image obtained from the diffraction spot marked as a circle in the diffraction pattern (**f**). **h** The Moire fringes can be observed at the disrupted region from a high-magnification TEM image. **i** The HRTEM image along the (110) zone axis in the disrupted region, revealing that the conductive filaments were converted back to ZnO_{1-x}. **j** The HRTEM of the "zinc" conductive filament along the (231) zone axis has been identified. **k** Solid-sphere model of ZnO in a wurtzite structure along the (110) zone axis. The coordinate lines are the unit cell vectors. **l** Solid-sphere model of zinc in a HCP structure along the (231) zone axis. The three-dimensional schematic illustrations of **m** a ZnO unit cell and **n** a zinc unit cell, respectively, showing that the zinc atoms position remain the same as the oxygen ions diffuse out [89]

91, 110, 136–152], and embedded/multilayered with various metalsor oxides [55, 83, 153–159].

According to electrochemical behavior of electrodes, the types of the electrodes that commonly stacked with storage material are inert, oxidizable, and active metals. Inert electrode, such as Pt, Ru, or Au, as a cathode may create high interface barrier to induce resistive switching properties [160]. High work function of these inert electrodes attributed to higher ON/OFF ratio [161]. As an anode, however, the high work function may not play important role; nonetheless, due to its inert behavior, the electrode has good electrochemical behavior that leads to efficient redox reaction [127]. Unfortunately, the preservation of oxygen in inert electrode is limited [37, 162, 163]. Unlike inert electrode, oxidizable metal electrode, as an anode, has an advantage of having oxygen reservoir behavior. This metal electrode tends to form thin interfacial metal oxide layer at top electrode (TE)/ZnO interface. The interfacial layer controls the oxygen outflow to the environment during SET process; thus the well-preserved oxygen leads to long endurance [164]. However, even though there are a number of oxidizable metal available, still, an appropriate anode for ZnO-based resistive memory needs to be selected carefully.

I-V switching characteristics of various metal top electrodes based having TE/ZnO/Pt structure is shown in Fig. 5a. Despite both Al and Cr are able to create AlO_x and CrO_xas oxygen reservoir at the interface, respectively, however, obvious device instability is exhibited in devices made with Al electrode, as shown in Fig. 5b, c.

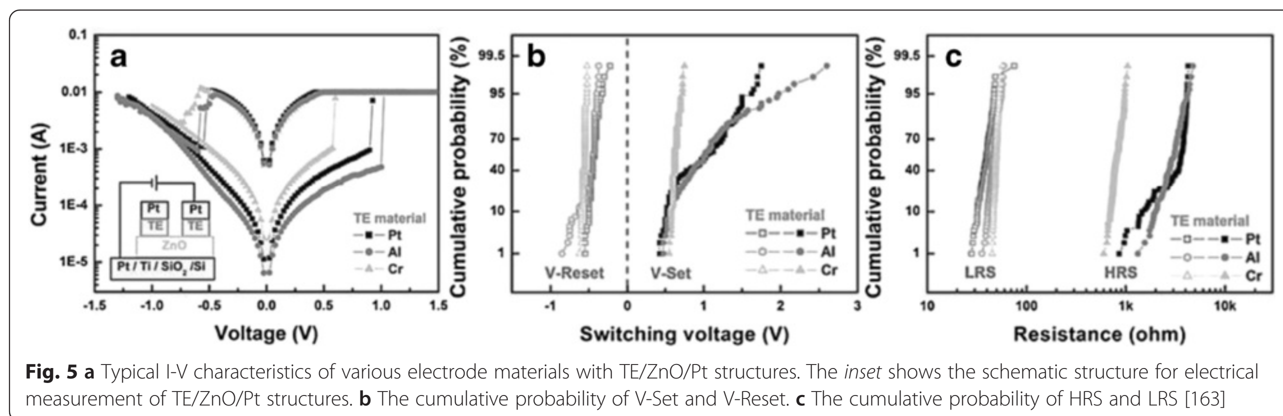

Fig. 5 **a** Typical I-V characteristics of various electrode materials with TE/ZnO/Pt structures. The *inset* shows the schematic structure for electrical measurement of TE/ZnO/Pt structures. **b** The cumulative probability of V-Set and V-Reset. **c** The cumulative probability of HRS and LRS [163]

Similar standard free energy of formation of oxide $\left(\Delta G_f^o\right)$ between Cr and Zn leads to efficient redox process [163]. Conversely, large difference ΔG_f^o between Al and Zn leads to less oxygen can be supplied from AlO_x to rupture the oxygen vacancies filament during reset process; in addition, the morphology of AlOx interface layer is found to be rough, which leads to device instability [163]. Hence, oxidizable metal having close ΔG_f^o with ZnO and smooth interfaces are crucial in selecting appropriate anode for reliable ZnO RRAM device [163, 165]. Among these three top electrodes (Cr, Al, and Pt), Cr top electrode shows better performance compared to others.

In ECM devices, however, the resistive switching behavior depends upon the electronegativity and ionic size of the active anodes which determine the mobility of metal cations inside ZnO [161]. The use of low electronegativity and small ionic size of the active anodes result in easier formation and rupture of CF in ECM devices compared to VCM devices [161]. Therefore, set and reset voltages in ECM are lower than that in VCM. Nevertheless, it is reported that a high electronegativity of Au may also behave as active metals [108]; in addition, the omission of Ni or Ag atoms diffusion in CF formation is also reported [166, 167]; this phenomena may relate to different ZnO film quality, device geometry, and operation method. The major device parameters as a function of different metal electrodes are summarized in Table 1. The best reported structures having a good combination between low power, endurance, and retention performance so far are Pt/ZnO/Pt [122] and Ag/a-ZnO/Pt [132] for VCM and ECM devices, respectively.

Effect of Deposition Parameter in ZnO-Based RRAM Devices

Besides electrodes, microstructural properties and defects in ZnO film strongly affect the switching behavior as well. Zinc interstitial and oxygen vacancy native defects behave as self dopants in pure ZnO [115, 116, 168]. Excessive defect concentration leads to high leakage current and degradation of device performance [169]. Controlled ZnO film growth is required in order to fabricate good quality film having highly oriented growth and less native defects. Several methods have been reported to fabricate high-quality ZnO film for RRAM application, such as ALD [133, 170–172], MOCVD [173], PLD [135], electrospray [125], electrodeposition [167], spin-coating [174], DC-sputtering [129, 131], and RF-sputtering [52]. Yet, sputtering is the most commonly used technique due to their thickness controllability, large area uniformity, low temperature, and less-toxic process. ZnO film properties can be simply controlled by modulating Ar/O_2 flow ratio during sputtering.

Figure 6 depicts the switching parameter of VCM and ECM unipolar devices made with various Ar/O_2 flow ratio. ON/OFF ratio tends to increase as oxygen flow ratio increase. ZnO grown on higher oxygen flow condition reduces the formation of oxygen vacancy defects which can generate more free carriers, thus leading to higher HRS resistance. In terms of device stability, as oxygen flow increases VCM, devices tend to be unstable. As oxygen flow increases, smaller grains are grown in the ZnO film that leads to higher number of grain boundaries and multiple conducting path [52], leading to unstability. Excessive conductive filaments result in unstable set/reset process in RRAM devices [54]. Conversely, higher oxygen flow results in better stability in ECM devices due to lower amount of pre-existing oxygen vacancy defects in ZnO film; thus, the electron conduction controlled by metallic bridge will be more dominant than the oxygen vacancies in ECM devices. Therefore, less reset competition between the metal bridge and oxygen vacancies during Joule heating process may lead to better stability. In addition, post-thermal treatment after deposition can also be employed to improve crystallinity and adjust the defect concentration in ZnO film. The decreasing of the native defects and increasing of crystallinity in ZnO film after air or oxygen ambient annealing may enhance ON/OFF ratio in ECM and VCM devices [134, 135]. Yet, this treatment may also increase the forming voltage; a high forming

Table 1 ZnO-based RRAM fabricated with various metal electrodes in published literature

No	Structure	CC (mA)	V_F (*V*)	V_R (*V*)	V_S (*V*)	Mode	Endurance (cycles)	ON/OFF ratio (times)	Retention (seconds)	Stress (seconds)	Memory type	Ref.
1	Pt/ZnO/Pt	30	~3.3	−1	~−2	U	100	10^3–10^4	NA	NA	VCM	[118]
2	Pt/ZnO/Pt	3	~4	~−0.5	~1.2	B	10^2/10^6(AC)	>10^2	>6×10^5/RT	NA	VCM	[122]
3	Pt/ZnO/Pt	NS	NS	−2.5	2.5	R	100	>40	NA	NA	VCM	[126]
4	Pt/ZnO/Pt	10	~4	~0.5	~1.5	U	200	58	9×10^4/RT	NA	VCM	[127]
5	Pt/ZnO/Ru	10	~4	~0.7	~1.9	U	200	175	9×10^4/RT	NA	VCM	[127]
6	Ru/ZnO/Pt	10	~4	~1	~2.1	U	200	61	9×10^4/RT	NA	VCM	[127]
7	TiN/ZnO/Pt	5	FF	~−1.2	~1.2	B	>500	10	NA	10^5/RT	VCM	[119]
8	Au/ZnO/ITO	SC	FF	~2	~−2	B	>10^2	>10	10^4/RT	NA	VCM	[120]
9	Al/ZnO/Al	1	NS	~0.5	~2.5	U	219	10^4	10^3	10^3/RT	VCM	[117, 121]
10	Al/ZnO/P++−Si	5	1.56	0.27	~1.41	U	>400	>10^3	NA	NA	VCM	[123]
11	TiN/ZnO/TiN	~80	FF	3	−4	B	NA	>10	10^4	NA	VCM	[133]
12	Ag/ZnO/Pt	10	FF	~−0.4	0.8	B	40	10^2	NA	10^4/RT	ECM	[124]
13	Ag/ZnO/Cu	NS	2.5	~−1.3	~1.3	B	>500	10^3	NA	NA	ECM	[125]
14	Cu/ZnO/ITO	NA	4.42	0.6	2.6	U	300	>20	NA	NA	ECM	[128]
15	Ag/a-ZnO/Pt	0.5	FF	−2	<0.5	B	100	10^7	10^6/RT	NA	ECM	[132]

Unless specified, endurance was measured using DC voltage sweeping mode

CC current compliance, V_F forming voltage, V_R reset voltage, V_S set voltage, *SC* self-compliance, *FF* forming free, *U* unipolar, *B* bipolar, *RT* measured at room temperature, *NA* data not available, *NS* not specified

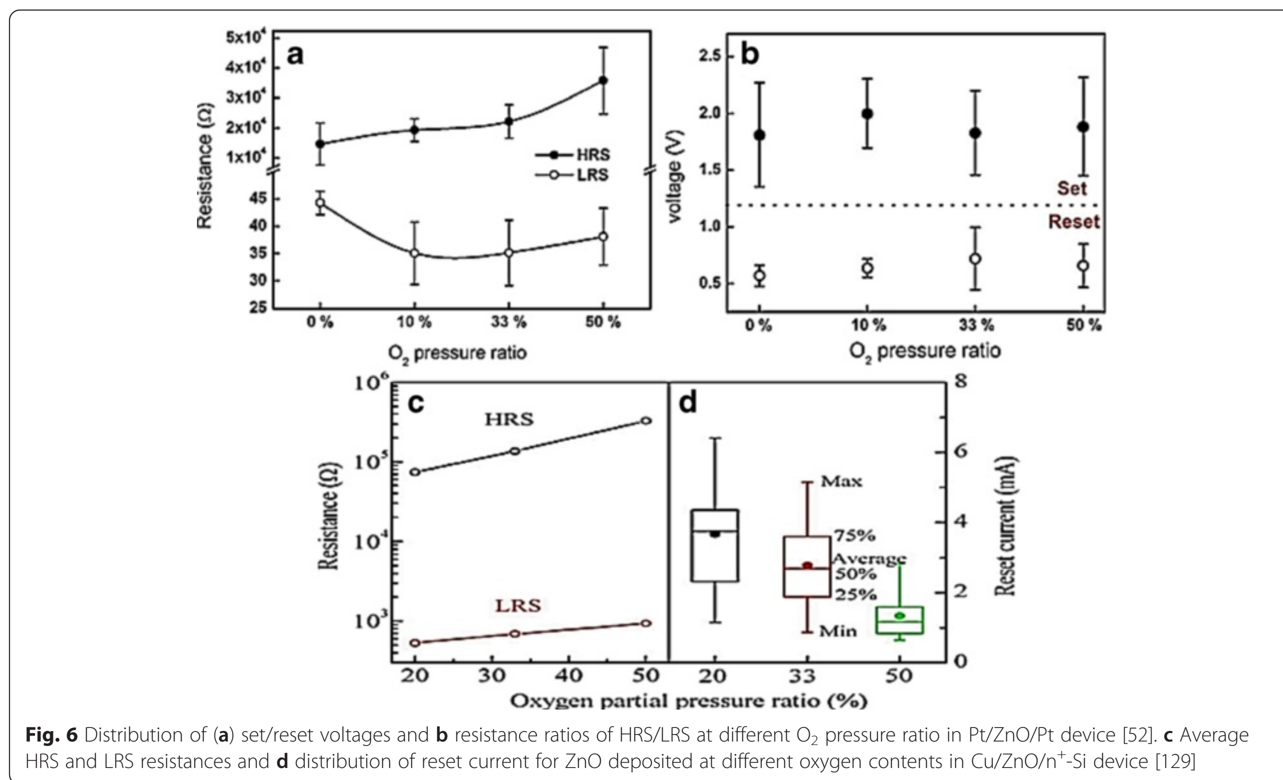

Fig. 6 Distribution of (**a**) set/reset voltages and **b** resistance ratios of HRS/LRS at different O_2 pressure ratio in Pt/ZnO/Pt device [52]. **c** Average HRS and LRS resistances and **d** distribution of reset current for ZnO deposited at different oxygen contents in Cu/ZnO/n^+-Si device [129]

voltage may generate large size and excessive number of CFs that may lead to switching instability [134, 135].

Besides Ar/O_2 flow ratio, switching layer thickness also plays a crucial role on the switching parameter in RRAM operation. Figure 7 shows the effect of ZnO thickness on the resistive switching performance of ECM and VCM unipolar devices [130, 131]. Higher forming voltage is required for thicker devices that are simply due to the longer CF that needs to be created between the electrodes. Reset voltage of VCM devices is insensitive to the thickness. However, Vset in VCM devices increases as ZnO thickness increases, due to higher crystallinity in thicker film. The higher crystallinity film having a larger grain size and lower density of dislocations may provide less conduction path during filament formation [130]. Contrarily, set and reset voltages of ECM devices are not directly affected by the structural properties due to oxide thickness. Similar phenomenon is also observed in doped ZnO bipolar ECM devices [146]. This phenomenon may arise due to the Joule heating effect taking place at a critical area where it is not significantly altered with the thickness variation [146]. It is also important to note that the

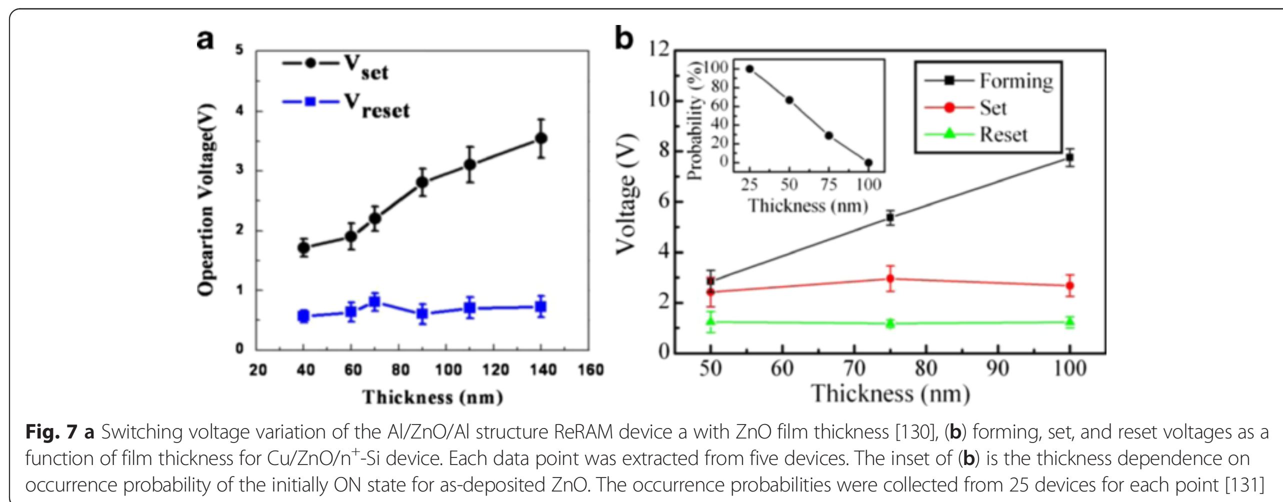

Fig. 7 **a** Switching voltage variation of the Al/ZnO/Al structure ReRAM device a with ZnO film thickness [130], (**b**) forming, set, and reset voltages as a function of film thickness for Cu/ZnO/n^+-Si device. Each data point was extracted from five devices. The inset of (**b**) is the thickness dependence on occurrence probability of the initially ON state for as-deposited ZnO. The occurrence probabilities were collected from 25 devices for each point [131]

improvement of ON/OFF ratio after slight adjustment in Ar/O_2 ratio or post-annealing treatment seems more obvious in VCM than ECM devices. Consequently, it opens another area and challenge on how to modulate the Joule heating effective region in ECM cell.

Effect of Doping in ZnO-Based RRAM Devices

Nevertheless, controlled deposition parameter and post-thermal treatment on resistive layer may be not as effective as doping technique to fully adjust the defect concentration. Various dopant elements, such as Al [137, 175, 176], B [177], Co [138, 139, 169, 178], Cr [110, 158], Cu [87, 140, 179], Fe [180, 181], Ga [112, 182, 183], La [144], Li [184, 185], Mg [55, 111, 145, 186–190], Mn [91, 146–148, 191–195], N [56, 149], Ni [196], S [197], Sn [90, 198], Ta [199], Ti [150, 151], V [85], and Zr [86], that have been reported may exhibit decent switching performance. ZnO-based RRAM with multi-element doping, such as Al-Sn [136, 200], Ga-Sn [201], and In-Ga [141–143, 202–208], is also proposed. The effect of doping on the resistive switching performance is summarized in Table 2. Among the reported devices, devices having Mn dopant exhibit not only good endurance but also long retention performance.

The concentration of native and extrinsic defects induced by doping can be efficiently tuned by considering the defect generation chemistry. The formation of native defects in nonstoichimetric ZnO can be expressed using Kroger-Vink notation as follows [169, 209]:

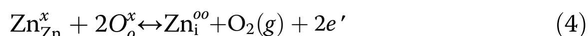

$$\mathrm{Zn}_{\mathrm{Zn}}^{x} + 2O_{o}^{x} \leftrightarrow \mathrm{Zn}_{\mathrm{i}}^{oo} + \mathrm{O}_2(g) + 2e' \quad (4)$$

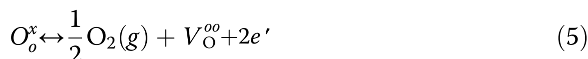

$$O_{o}^{x} \leftrightarrow \frac{1}{2}\mathrm{O}_2(g) + V_{\mathrm{O}}^{oo} + 2e' \quad (5)$$

where $\mathrm{Zn}_{\mathrm{Zn}}^{x}$ and $\mathrm{Zn}_{\mathrm{i}}^{oo}$ are a neutral charge of a Zn ion in a zinc site and a doubly positive charge of a Zn ion in an interstitial site, respectively. Excessive $\mathrm{Zn}_{\mathrm{i}}^{oo}$ and V_{O}^{oo} concentration may deteriorate switching performance [145, 169]. Therefore, the purpose of ZnO doping is to promote compensator defects and to decrease the native defect concentration. For example, the formation of compensator defects due to Co dopant can be expressed using Kroger-Vink notation as follows [169, 209]:

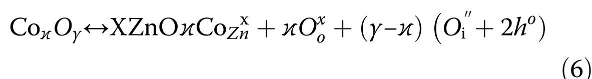

$$\mathrm{Co}_{\varkappa}O_{\gamma} \leftrightarrow \mathrm{XZnO}\varkappa\mathrm{Co}_{Zn}^{x} + \varkappa O_{o}^{x} + (\gamma - \varkappa)\left(O_{\mathrm{i}}^{''} + 2h^{o}\right) \quad (6)$$

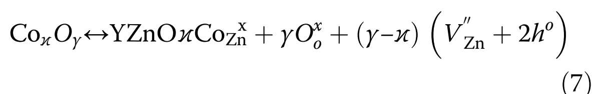

$$\mathrm{Co}_{\varkappa}O_{\gamma} \leftrightarrow \mathrm{YZnO}\varkappa\mathrm{Co}_{\mathrm{Zn}}^{x} + \gamma O_{o}^{x} + (\gamma - \varkappa)\left(V_{\mathrm{Zn}}^{''} + 2h^{o}\right) \quad (7)$$

where $\mathrm{Co}_{\mathrm{Zn}}^{x}, O_{i}^{''}, V_{\mathrm{Zn}}^{''}$, and h^{o} are a neutral charge of Co ion in a Zn site, a doubly negative charge of an O ion in an interstitial site, a doubly negative charge of a Zn vacancy, and a singly positive charge of a hole, respectively. As the result, oxygen concentration and insulating behavior in resistive layer are increased and thus improve ON/OFF ratio [169]. However, excessive dopant may deteriorate switching cycles and stability performance [110, 143, 151, 169, 175, 179, 190]. The deterioration occurs due to the weakening of c-axis-textured structure after increasing dopant concentration [169].

C-axis texture is a beneficial characteristic of ZnO that plays an important role to confine CF [127]. Figure 8 shows the schematic of CF development in various concentration of Co-doped ZnO resistive layer [169]. The study suggests there is a trade-off in reducing native defects and maintaining c-axis-textured structure in ZnO-based RRAM [169]. Therefore, the trade-off should be well adjusted for achieving a decent endurance performance.

It can also be noted that such trade-off may limit the fabrication of fully c-axis-textured growth. Consequently, the "hunt" for finding suitable doping element and technique that allow the increasing of both acceptor defects and microstructural quality is still needed. Employing a p-type doping element such as nitrogen may increase both acceptor concentration and microstructural quality, thus improving RRAM performance [56, 149]. In addition, p-type ZnO-based RRAM still has not received sufficient attention yet.

Employing an amorphous resistive layer may also avoid the formation of excessive and branching of CF due to the lack of grain boundary structure. Several efforts have been reported to fabricate amorphous ZnO-based RRAM, such as by doping [90, 141–143, 177, 198, 201–203, 205–208], hydrogen peroxide treatment [183], and deposition parameter optimization [132].

ZnO-Based Complementary RRAM

Although doping technique can be considered as the simplest way to improve switching properties, embedded and multilayered structure still receive great attention due to easy modulation of switching behavior in the switching layer. Table 3 shows the summary of the important switching parameters of multilayered and embedded ZnO-based RRAM. Multilayer structure can be employed not only to improve switching performance but also to generate different peculiar switching characteristics. By employing proper electrical programming to control formation and rupture of CF at the particular switching layer, complementary switching (CS) characteristics can be achieved. CS is a unique switching characteristic that is useful for avoiding sneak path disadvantage in a three-dimensional crossbar RRAM application [153, 154].

Figure 9a shows the CS characteristic of TiN/MgZnO/ZnO/Pt double layer memory device [153]. The CS characteristic can be obtained under proper programming

Table 2 Doped ZnO-based RRAM in published literature

No	Structure	CC (mA)	V_F (V)	V_R (V)	V_S (V)	Mode	Endurance (cycles)	ON/OFF ratio (times)	Retention (seconds)	Stress (seconds)	Ref.
1	Cu/N:ZnO/Pt	10	NS	~−0.45	~1.47	B	100	$>10^2$	NA	NA	[56]
2	$Ag/Zn_{0.98}Cu_{0.02}O/ITO$	10	NS	~−0.02	1.8	B	NA	10^6	$<10^3$	NA	[87]
		1	NS	−3.5	−15	U	NA	10^4	$>10^3$	NA	
3	Pt/ZnVO/Pt	10	~−4	~−0.5	~−2.5	B	10^5	$\sim10^2$	36×10^3/85 °C	NA	[85]
4	$Pt/Zn_{0.99}Zr_{0.01}O/Pt$	1	~−2	~1	~−1.5	B	10^4	$\sim10^2$	NA	NA	[86]
5	Al/ZTO/Pt	5×10^{-4}	~−2	~1	~−2.5	B	50	1.4×10^3	10^4/RT	NA	[90]
6	Pt/Mn:ZnO/Si	NS	FF	~−20	~20	B	45×10^2	$\sim 10^3$	5×10^3/RT	NA	[91]
7	$Pt/Zn_{1-x}Cr_xO/Pt$	–	FF	~3.5	~3	B	100	7×10^3	36×10^3/RT	NA	[110]
8	Ti/AZTO/Pt	3	NS	~1.6	~1.1	B	256	18	NA	10^4	[136]
9	Au/Co-ZnO/ITO/Au	–	FF	4	2.6	BS	4000	~7	NA	NA	[138]
10	Pt/Co:ZnO/Pt	10	FF	~−1	1.5–3	B	300	10^2	NA	NA	[139]
11	Al/ZnO:Cu/Pt	10	~12	~0.5	~2	U	450	470	10^4/RT	NA	[140]
12	TiN/Ti/IGZO/Pt	10	~6	~−1.5	~1	B	10^4	~10	NA	NA	[141]
13	Pt/a-IGZO/Pt	10	~10	~−1	~1.5	B	100	>10	$>10^4$/RT	NA	[142]
14	Al/IGZO/Al	–	~5	~5	~−5	B	100	~2	NA	NA	[143]
15	Pt/ZnLaO/p-Si	10	~6	~1	~2.5	U	150	>10	10^6	NA	[144]
	Pt/ZnLaO/Pt	10	~4	~0.5	~2.5			$>10^3$		NA	
16	$Pt/(Zn_{1-x}Mg_x)O/Pt$	10	~5	~1.5	~3.5	U	50	$140–10^3$	NA	NA	[145]
17	Cu/ZnO:Mn/Pt	5	~1.9	~−0.6	~1.2	B	65	$>10^3$	10^4/85 °C	NA	[146]
18	$Au/ZnMn_2O_4/Pt$	1	NS	~2	~10	U	8000	$10^5–10^7$	4×10^4/RT	NA	[147]
	$Au/ZnMnO_3/Pt$							$10^4–10^5$			
19	$Pt/Mn:ZnO_xS_{1-x}/Cu$	NS	NS	~0.5	1–3	U	100	$10^5–10^6$	10^4/RT	NA	[148]
20	Au/Cr/ZnO:N/TiN	5	2.5	~−1	~0.75	B	100	~1	10^4/RT	NA	[149]
21	Au/Ti:ZnO/ITO	–	FF	~−3	~3	B	200	14	2×10^3/RT	NA	[150]
22	Pt/ZnO:Ti/n+–Si	10	~5.5	~1	2–4	U	200	$>10^2$	$>10^5$/RT	NA	[151]
23	Ag/ZnO:Mn/Pt	SC	FF	−2.6–−0.5	0.3–3.8	B	100	10^7	$>10^7$/RT	NA	[152]
24	$Al/GaZnOx/p^+$-Si	7	~4.8	~−2.8	~3.5	B	100	10^2	NA	NA	[183]
25	$Ti/Mg_{0.1}ZnO_{0.9}/Pt$	1	FF	−1.5	1.5	B	500	$>10^3$	10^4	NA	[189]

NS not specified, *CC* current compliance, *SC* self-compliance, *FF* forming free, *U* unipolar, *B* bipolar, *BS* bistable, *VF* forming voltage, *VR* reset voltage, *VS* set voltage, *RT* measured at room temperature, *NA* data not available

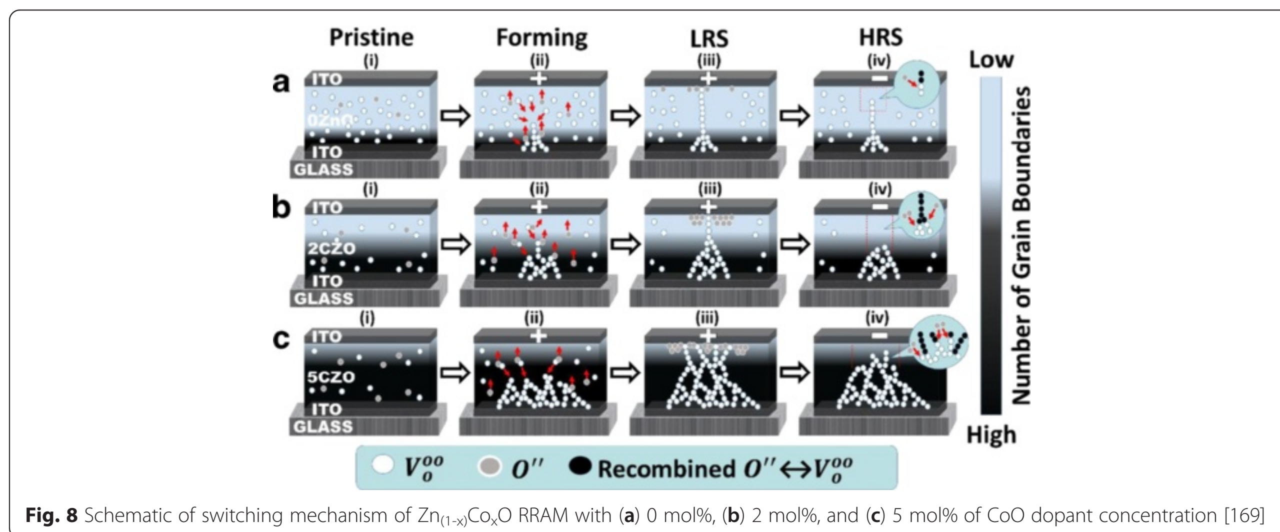

Fig. 8 Schematic of switching mechanism of $Zn_{(1-x)}Co_xO$ RRAM with (**a**) 0 mol%, (**b**) 2 mol%, and (**c**) 5 mol% of CoO dopant concentration [169]

steps, which can vary from device to device. For the TiN/MgZnO/ZnO/Pt memory device structure, the programming steps are as follows [153]: firstly, the device is operated under common counterclockwise bipolar switching mode. When the device is on LRS (set), low negative bias of −1 V was applied on top electrode (TE); consequently, oxygen vacancies move toward the MgZnO layer, by leaving some filament gap in the ZnO layer and make the device in HRS (reset). This process is called second electroforming. When low positive bias of ~0.6 V is applied on TE (V_{th1}), the oxygen vacancies repulse back to ZnO layer and resulted both layers in LRS (set); however, as the bias is continuously applied to reach ~1 V (V_{th2}), the oxygen vacancy filament size at MgZnO layer is reduced and ruptured. Similarly, the same mechanism may apply with the negative bias. Low negative bias of ~−0.6 V (V_{th3}) may repulse the oxygen vacancies from ZnO layer to MgZnO layer and form the filament at the MgZnO layer; consequently, both layers are in LRS (set). As the negative bias is continuously applied to reach ~−1 V (V_{th4}), the oxygen filament size at ZnO layer is gradually ruptured and makes the device back to HRS (reset) [153].

Another method to produce CS characteristic is by simply reversely stacking two cell memories. Figure 9b, c shows the resistive switching characteristics of Pt/ZnO/ZnWOx/W (cell A) and W/ZnWOx/ZnO/Pt (cell B) memory, respectively [154]. These devices can only be set (LRS) and reset (HRS) by applying negative and positive bias at the Pt electrode, respectively. Figure 9d shows the CS characteristics of Pt/ZnO/ZnWOx/W/ZnWOx/ZnO/Pt device [154]. The CS characteristic on this device can be generated under programming steps as followed [154]; initially, both cells are in HRS, called

Table 3 Multilayered and embedded ZnO-based RRAM in published literature

No	Structure	CC (mA)	V_F (V)	V_R (V)	V_S (V)	Mode	Endurance (cycles)	ON/OFF ratio (times)	Retention (seconds)	Stress (seconds)	Ref.
1	Pt/ZnO/$Ag_{0.2}$-$Al_{0.8}$/Al	1	NS	~0.3	~2	U	200	>10^2	NA	NA	[53]
2	TiN/MgZnO/ZnO/Pt	10/20	~6	−2	~1	B	10^4	>50	3×10^4/RT	NA	[55]
3	Pt/ZnO/ZrO_2/Pt	10	~−6.5	−4	~3	B	100	~5	NA	10^4	[83]
4	Pt/ZnO/CoOx/ZnO/Pt	10	FF	0.8–1.8	1.5–2.9	B	200	~10^2	NA	NA	[155]
5	Pt/ZnLaO/ZnO/Pt	10	~3.5	~1	~2.3	U	100	~10^4	10^4/65 °C	NA	[156]
6	Ag/CeO_2/ZnO/NSTO	10	NS	−5	~2	B	100	540	10^3/RT	NA	[157]
7	Pt/ZnO/Cr/ZnO/Pt	NS	~2	−2	3	B	10^4	~10^4	NA	5×10^3	[158]
8	Pt/$(ZnO/Ti/ZnO)_{1-4}$/ITO	NS	FF	~−2.5	~2	B	320	~10^3	>10^6	NA	[159]
9	Ag/GZO/ZnO/Pt/Ti	10	FF	0.55	0.4	B	~40	2×10^3	1.1×10^4	NA	[182]
10	Pt/TiO_x/ZnO/n^+-Si	NS	~2.8	~0.5	~2	U	>50	>10^2	NA	NA	[286]
11	Al/Al_2O_3/(ZnO/Al_2O_3) 10/n-Si/Al	NS	FF	−7	7	B	NA	10^3–10^4	10^3	NA	[287]

NS not specified, *CC* current compliance, *FF* forming free, *U* unipolar, *B* bipolar, *VF* forming voltage, *VR* reset voltage, *VS* set voltage, *RT* measured at room temperature, *NA* data not available

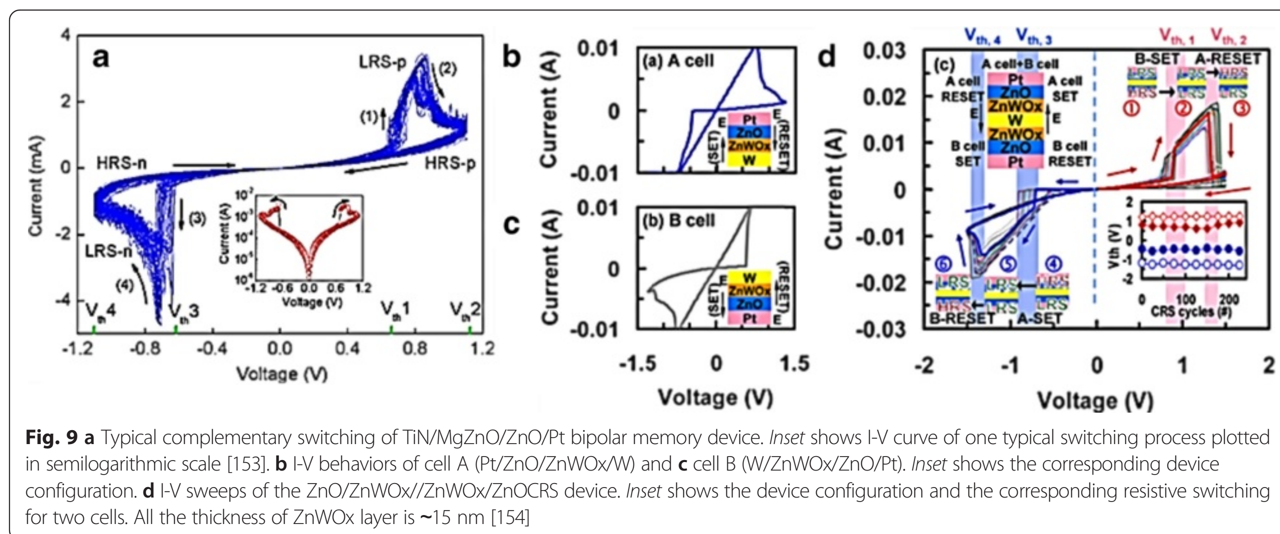

Fig. 9 **a** Typical complementary switching of TiN/MgZnO/ZnO/Pt bipolar memory device. *Inset* shows I-V curve of one typical switching process plotted in semilogarithmic scale [153]. **b** I-V behaviors of cell A (Pt/ZnO/ZnWOx/W) and **c** cell B (W/ZnWOx/ZnO/Pt). *Inset* shows the corresponding device configuration. **d** I-V sweeps of the ZnO/ZnWOx//ZnWOx/ZnOCRS device. *Inset* shows the device configuration and the corresponding resistive switching for two cells. All the thickness of ZnWOx layer is ~15 nm [154]

as "OFF" state. Then, one of the cells (cell A) is switched to LRS while cell B can be maintained in HRS by sweeping low negative bias at the TE. At this stage, cell B is still in HRS because it requires the opposite bias to switch and act as a voltage divider. As the positive sweep bias reach ~0.9 V (V_{th1}), cell B is switched to LRS. Because the positive bias of ~0.9 V is not enough to switch the cell A from LRS to HRS, therefore at this stage, both cells are in LRS. When both cells are in LRS, it is called as "ON" state. Further increase of positive bias to ~1.3 V (V_{th2}) leads to reset cell A. At this stage, cells A and B are in HRS and LRS, respectively, called as "1" state. In order to switch the device back to "ON" state, cell A needs to switch back to LRS by sweeping with negative bias of ~−0.6 V (V_{th3}); therefore, both cells are in LRS. Similarly, at this stage, cell B can still maintain its LRS because ~−0.6 V is not enough to switch it to HRS. However, as the sweep negative bias continues to reach ~−1.3 V (V_{th4}), cell B is switched to HRS. Therefore, at this stage, cells A and B are in LRS and HRS, respectively, called as "0" state. Consequently, four distinct threshold biases can be applied to obtain CR switching characteristics [154].

Achieving CS by employing the above methods is very useful to maintain simplicity of the memory structure and fabrication. Yet, further investigation is necessary to expand the potential of these methods for ZnO-based ECM cell and transparent VCM cell.

ZnO-Based Transparent/Flexible RRAM

Nonvolatile memory structure having high transmittance in visible light would be useful for the realization of fully integrated transparent electronics [210, 211]. Employing wide direct band gap switching materials, transparent conducting oxide (TCO) electrodes, and transparent substrate is required to construct invisible RRAM structure. ITO [54, 176, 212–220], FTO [213], AZO [54, 219, 221], and GZO [222–224] are the commonly used TCO as electrodes for transparent electronics. Conduction and interfacial growth properties of TCO are strongly determined by its fabrication parameter. However, still few investigations have been conducted to explain phenomena in RRAM operation due to different properties of TCO [219, 225–227].

High quality of ZnO resistive switching layer was deposited on TCO electrodes using various methods, such as metal organic chemical vapor deposition (MOCVD) [212, 223, 224], pulsed laser deposition [213, 218, 221, 222], RF-sputtering [54, 176, 216, 217, 219], hydrothermal growth [216], and sol-gel [214, 215, 220]. Figure 10a–c demonstrates sol-gel-derived ITO/GZO/ITO RRAM devices on glass substrate. The device is fully transparent (~80 %) in the visible region as shown in Fig. 10d. Devices with an average transparency of above 70 % in visible light region can be considered as having transparent structure, while semi-transparent is below 70 % [228]. Table 4 summarizes the switching parameters and performances of the ZnO-based transparent RRAM (TRRAM). Multilayer devices made of GZO/Ga_2O_3/ZnO/Ga_2O_3/GZO structures exhibit the highest transparency with high memory window and long retention performances [223].

By taking an advantage of low synthetic temperature of ZnO material, it allows us to fabricate flexible RRAM (FRRAM) devices on polymer substrate. Flexible nonvolatile memory may revolutionize electronics due to its potential in embedded flexible technologies [229]. Polyethylene terephthalate (PET) [220, 230, 231], polyethylene naphthalate (PEN) [113], polyethersulfone (PES) [232, 233], polymide (PI) [234], and Kapton [235] are commonly used as polymer substrate; however, flexible RRAM, but not transparent, having metal foil [236] and stainless steel [237]

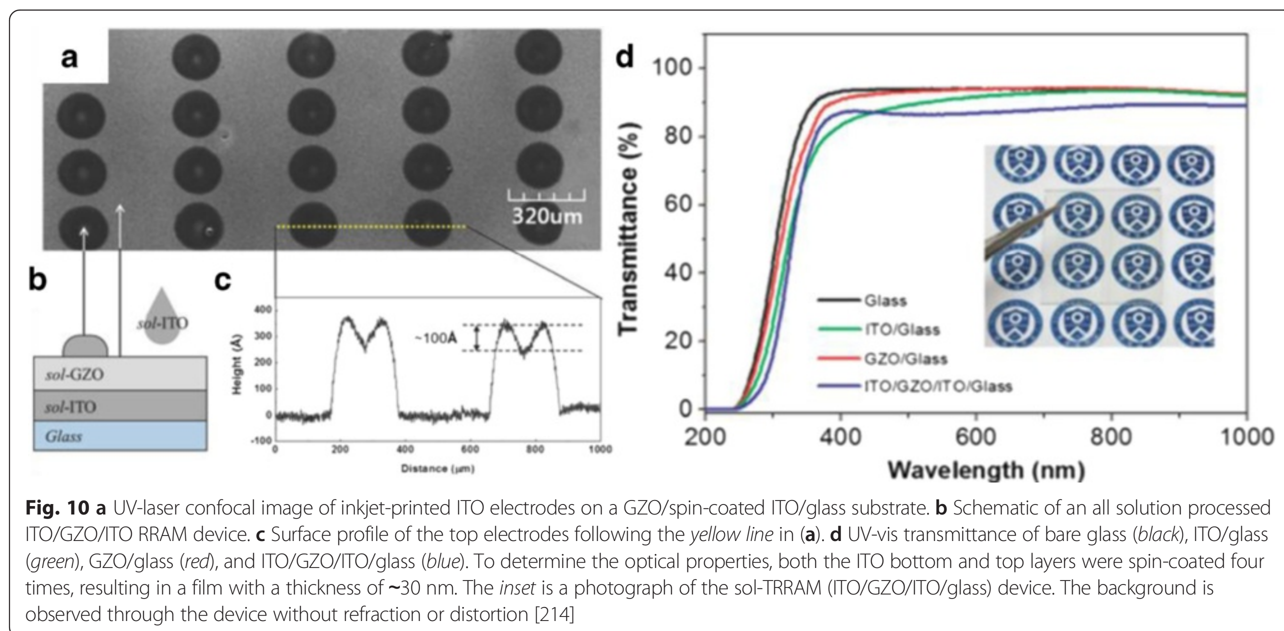

Fig. 10 **a** UV-laser confocal image of inkjet-printed ITO electrodes on a GZO/spin-coated ITO/glass substrate. **b** Schematic of an all solution processed ITO/GZO/ITO RRAM device. **c** Surface profile of the top electrodes following the *yellow line* in (**a**). **d** UV-vis transmittance of bare glass (*black*), ITO/glass (*green*), GZO/glass (*red*), and ITO/GZO/ITO/glass (*blue*). To determine the optical properties, both the ITO bottom and top layers were spin-coated four times, resulting in a film with a thickness of ~30 nm. The *inset* is a photograph of the sol-TRRAM (ITO/GZO/ITO/glass) device. The background is observed through the device without refraction or distortion [214]

substrates, was also reported. Figure 11a shows the typical photograph of flexible RRAM having Al/ZnO/Al structures fabricated on PES substrate.

Mechanical flexibility is the essential consideration for flexible memory application feasibility. Reliable memory window and endurance should be maintained in various bending condition and after repetitive flexes. Mechanical parameter related to tensile and compressive strain that were given upon a memory structure should be taken into account. Figure 11b shows the schematic illustration of a flexible substrate receiving tensile and compressive strain. The strain induced on the surface of a substrate due to bending can be calculated using Eq. 8 [238];

$$S = \frac{(t_L + t_S)(1 + 2\eta + x\eta^2)}{2R(1+\eta)(1+x\eta)} \quad (8)$$

where S is strain, $\eta = t_L/t_S$, t_L is layer thickness, t_S is substrate thickness, $\chi = Y_L/Y_S$, Y_L is the Young's modulus of the layer, and Y_S is the Young's modulus of the substrate. Nevertheless, there is no definite standard or apparatus for mechanical flexibility test on RRAM; yet, HRS and LRS values recorded at different bending radius and repeated bending are generally conducted to measure the memory flexibility.

Employing metal as bottom electrode may help mechanical flexibility of FRRAM due to its higher ductility properties as compared to oxide electrode. Nonetheless, having TCO as electrodes is unneglectable when fabricating transparent and flexible RRAM (TFRRAM). TCO films fabricated on flexible substrate may suffer from cracking after repeated bending. Related to that, compressive stress results more damage to the films than tensile stress [239]. In order to minimize this issue, inserting thin metal between TCO layers has been suggested [233].

Figure 12 shows flexibility test of ITO/ZnO/ITO/PES and ITO/ZnO/ITO/Ag/ITO/PES TFRRAM. Both devices have shown stable states in various bending radius, as shown in Fig. 12a. However, devices having single layer ITO bottom electrode suffer HRS and LRS degradation upon repeated bending; conversely, devices having ITO/Ag/ITO multilayer bottom electrode exhibit excellent stability. However, inserting thin metal film between TCO layers may decrease its transparency [233] and increase the cost of production process [239]. Another method to enhance bending durability of films while maintaining the transparency is by employing TCO/oxide buffer layer/flexible substrate structure [239].

Nonetheless, mechanical flexibility of FRRAM can rely on not only the ductility of the bottom electrode but also the resistive layer as well. Interestingly, Al/GOZNs/ITO/PET FRRAM devices are able to maintain its states after repeated bending with extreme bending radius of 6 mm [230]. This may suggest that the excellent mechanical flexibility of the FRRAM may also be attributed from the ZnO nanorods-graphene oxide composite resistive layer ductility. Recent report also implied that employing amorphous InGaZnO (α-IGZO) as a resistive layer may exhibit better mechanical flexibility than polycrystalline oxide resistive layer [240]. Yet, further investigation is necessary to explain the influence of ZnO microstructural properties on resistive switching performance under various bending condition. The switching parameters of the flexible resistive switching memory along with flexibility are summarized in Table 5.

Table 4 ZnO-based transparent RRAM in published literature

No	Structure	%T	Mode	CC (mA)	V_F (V)	V_R (V)	V_S (V)	Endurance (cycles)	ON/OFF ratio (times)	Retention (s/°C)	Ref.
1	AZO/ZnO_{1-x}/ITO	~85	B	1	−5.5/4 (DF)	−2	~1.7	>450	~10^2	10^4/RT	[54]
2	ITO/$Zn_{0.98}Co_{0.02}O$/ITO	90	B	5	3	−1.5	1.2	5000	15	NA	[169]
3	ITO/AZO/ITO	~81	B	10	~2.3	~−0.5	~0.5	300	3	NA	[176]
4	ITO/ZnO/ITO	81	U	15	3.2	1.8	2.6	10^2	~10^2	10^5/RT	[212]
5	ITO/ZnO:Mg/FTO	80	B	50	2.8	−3	1.8	10^5	2.5	5×10^3/110 °C	[213]
6	ITO/GZO/ITO	~86.5	B	0.1	FF	−7	6	350	15	NA	[214]
7	ITO/GZO-nanorods/ZnO/ITO	~80	B	10	~3	~−2	~2	>7000	>200	10^4/85 °C	[216]
8	ITO/graphene/ZnO/ITO	75.6	B	5	4	~−2.5	~1	100	20	10^4/RT	[217]
9	ITO/ZnO/$Pr_{0.7}Ca_{0.3}MnO_3$/ITO	79.6	B	10	FF	~2	~−2	2.5×10^3	10^4	NA	[218]
10	AZO/ZnO/ITO	~80	B	10	~3.5	−2	~1.5	10^4	14	NA	[219]
12	AZO/MZO/AZO	64–82	B	1	−6	~−4	~3	50	3	10^5/RT	[221]
13	GZO/ZnO/GZO	~80	U	10	3.5	~1.6	~2.2	7	~5	NA	[222]
14	GZO/Ga_2O_3/ZnO/Ga_2O_3/GZO	92	B	20	FF	−12	14	50	10^2	10^5/RT	[223]
15	ITO/IGZO/ITO	70–80	B	10	FF	3.5	~−1	10^2	32	10^4/RT	[288]

%T percentage of transmittance in visible range, *U* unipolar, *B* bipolar, *CC* current compliance, *FF* free forming, V_F forming voltage, V_R reset voltage, V_S set voltage, *DF* double forming, *RT* measured at room temperature, *NA* data not available

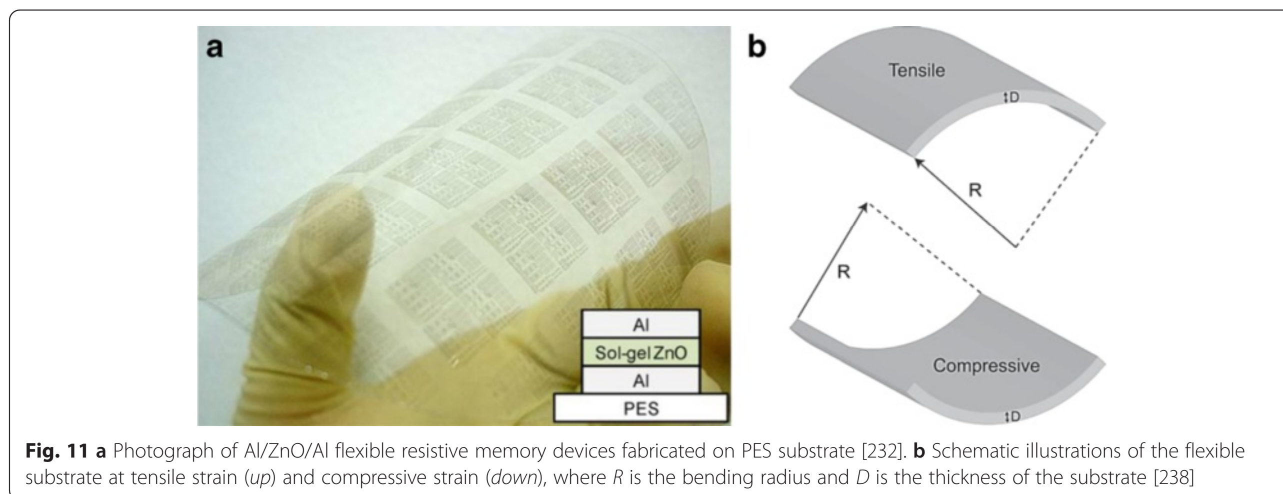

Fig. 11 a Photograph of Al/ZnO/Al flexible resistive memory devices fabricated on PES substrate [232]. **b** Schematic illustrations of the flexible substrate at tensile strain (*up*) and compressive strain (*down*), where *R* is the bending radius and *D* is the thickness of the substrate [238]

Sneak Current Prevention in ZnO-Based RRAM

To resolve the physical scaling issues of conventional nonvolatile memory devices, crossbar array architecture has been considered as an attractive construction due to the scalability, simplicity, and multiple stackability of the structure. For practical applications, the foremost bottleneck of this array architecture is the sneak current path issue, which leads to read operation error [241]. ZnO-based RRAM having crossbar structures has also suffered from sneak path issue. To suppress the undesired sneak current, the combination of memory cells with rectifying or switch devices, such as p-n junction diodes [242], Schottky diodes [243, 244], threshold switching devices [245], and transistors [246], is necessary. In this section, we will discuss about the different aspects to eliminate sneak path for the ZnO-based RRAM.

Seo et al. [247] reported ZnO crossbar Pt/ZnO/Pt resistive random access memory stacked with heterostructure diodes of Pt/NiO/ZnO/Pt p-n junction and the Pt/WO_3/ZnO/Pt tunnel barrier diodes for eliminating the sneak current effect to avoid sneak path current, as shown in Fig. 13. The fabricated ZnO RRAM device on glass with a 4 × 4 crossbar array stacked with heterostructure diodes is shown in Fig. 13a. Cross-sectional TEM images of the stacked contact area of different diodes is presented in Fig. 13b. Figure 14a, b reveals the current characteristics of the crossbar array ZnO RRAM devices combined with the heterostructure diodes. Inset shows the corresponding energy band diagram of the diodes. Stable resistive switching occurring with larger operation voltages is observed due to the additional series resistance of the heterostructure diodes. However, the reverse current was effectively suppressed by combining with the diodes. Similar behavior is also reported by employing vertically integrated Ag/MgZnO/GaZnO/Au Schottky diode on Au/FeZnO/MgO/Pt RRAM device [248]. Usually, diode or transistor or selector needs to be combined with the RRAM resistor to avoid sneak path current. But, recently, Fan et al. avoided sneak path current by fabricating selector-less AZTO-based RRAM

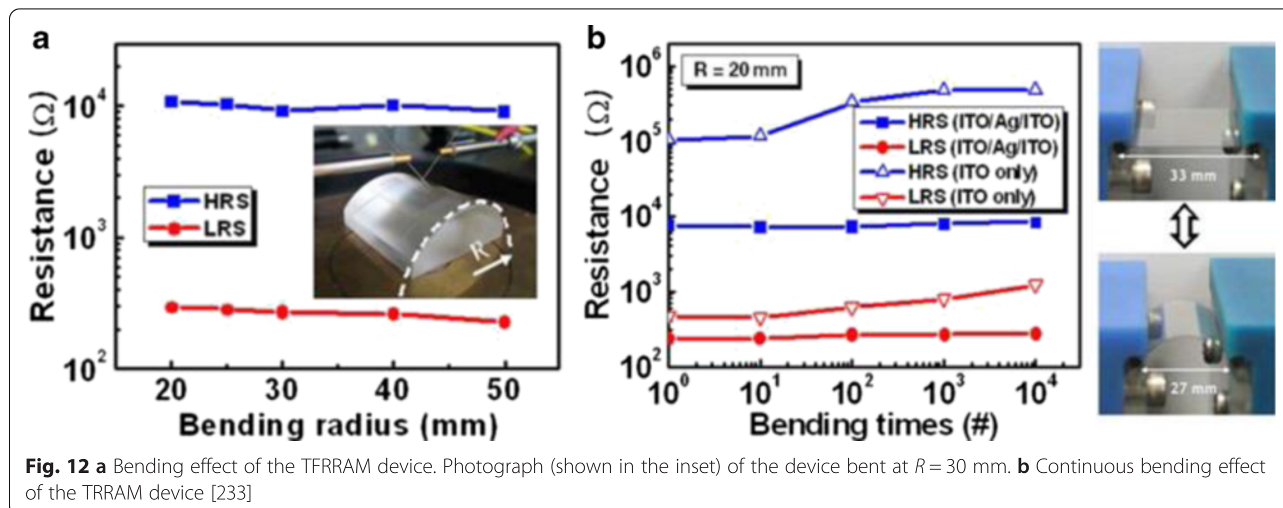

Fig. 12 a Bending effect of the TFRRAM device. Photograph (shown in the inset) of the device bent at *R* = 30 mm. **b** Continuous bending effect of the TRRAM device [233]

Table 5 ZnO-based flexible RRAM in published literature

No	Structure	%T	Mode	CC (mA)	V_F (V)	V_R (V)	V_S (V)	Endurance (cycles)	ON/OFF ratio (times)	Retention (s/°C)	Stress (s)	Flexibility test			Ref.
												Bending cycles (times)	Radii (mm)	ON/OFF ratio (times)	
1	GZO/GZO(H)/GZO/PEN	66	B	0.1	~1.7	−2	~1.5	20	20	NA	NA	NA	NA	NA	[113]
2	Ag/ZnO/ITO/PET	NT	B	SC	NS	3 – 4.9	−0.7−−3.2	>100	>60	$>4 \times 10^3$/RT	NA	2400	8	~10	[220]
3	Al/GOZNs/ITOPET	NT	B	2	NS	−2	2.1	200	$\sim10^2$	10^4/RT	NA	10^3	6	$\sim10^2$	[230]
4	Cu/ZnO:Mg/ITO/PET	NT	B	1	2.6	~−1.5	~ 1	100	30	144×10^2/RT	NA	10^3	20	30	[231]
5	Al/ZnO/Al/plastic	NT	U	5	FF	~0.5	~2	10^4	10^4	NA	10^5	10^5	NS	~10	[232]
6	ITO/ZnO/ITO/Ag/ITO/PES	80	U	10	3.4	0.6	1.5	200	>10	10^5/85 °C	NA	10^4	20	>10	[233]
7	Au/ZnO NR/Au/PI	NT	U	50	~1.7	0.23 ± 0.02	0.84 ± 0.04	>100	10	10^4/RT	NA	100	20	~10	[234]
8	Al/Mn:ZnO/HfO_2/Ti/Pt/Kapton	NT	B	NS	NS	−5	5	50	70	NA	500	500	11	~70	[235]
9	Au/ZnO/Stainless steel	NT	NP	30	NS	±0.5–0.8	±1.0–2.0	100	10^2	NA	NA	NA	NA	NA	[237]
10	Cu/α-IGZO/Cu/plastic	~65	U	3	FF	~0.5	~1.5	150	10^2–10^3	NS	NA	10^5	NS	10^2	[240]

%T percentage of approximate transmittance in visible range, *NT* not transparent, *NP* nonpolar, *CC* current compliance, *U* unipolar, *B* bipolar, *SC* self-compliance, *FF* free forming, *Vf* forming voltage, *Vr* reset voltage, *Vs* set voltage, *RT* room temperature, *NS* not specified, *NA* not available

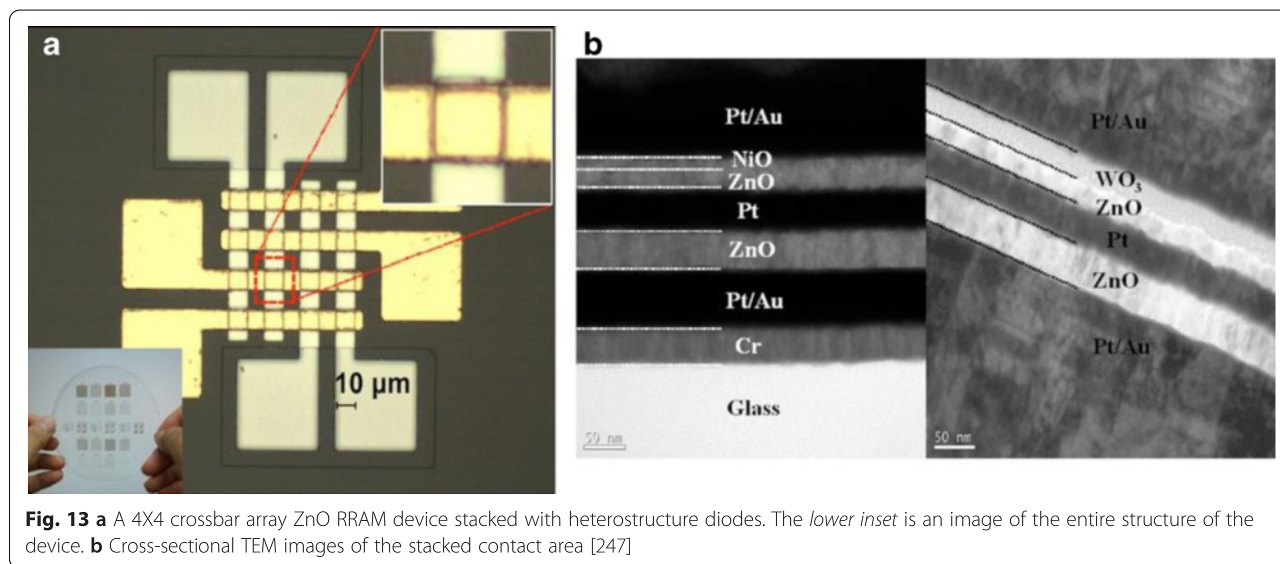

Fig. 13 **a** A 4X4 crossbar array ZnO RRAM device stacked with heterostructure diodes. The *lower inset* is an image of the entire structure of the device. **b** Cross-sectional TEM images of the stacked contact area [247]

with a thin insertion layer (2 nm) of Al_2O_3 [200]. Figure 15a, b shows typical cross-section TEM image of Ti/AZTO/Al_2O_3/Pt and the schematic of the fabricated device, respectively [200]. This device is able to exhibit read margin with inhabit ratio (IR) of 34 times, as depicted in Fig. 15c, d [200]. They suggested that Al_2O_3 may act as an electron barrier where the LRS conduction is dominated by electron tunnelling mechanism [200].

Nanostructured ZnO-Based RRAM

To reduce the production cost, highly densed RRAM can be achieved with a maximum size of $4F^2$ high packing density by stacking architecture via three-dimensional crossbar [43, 154, 249]. However, further effort to scaling down the memory size using unique structure, such as self-assembly nanostructure, is very attractive. The wide variety of ZnO morphologies offers novel approach and understanding to dimensionality dependence on switching characteristics. Currently, devices employing nanorods/nanowires [58–75, 216, 250–266], nanobelts [76], and nanoisland [77, 78] as the switching elements receive considerable interests in developing one-dimensional resistive memory for ultrahigh density memories.

Figure 16a, b shows the schematic of Pt/ZnO_{1-x} nanorods/ZnO/Pt device and the cross-sectional SEM image, respectively [256]. It is believed that ionic defects prefer to diffuse through the nanorods sidewall due to higher microstructural defects [252, 253]. Thus, the

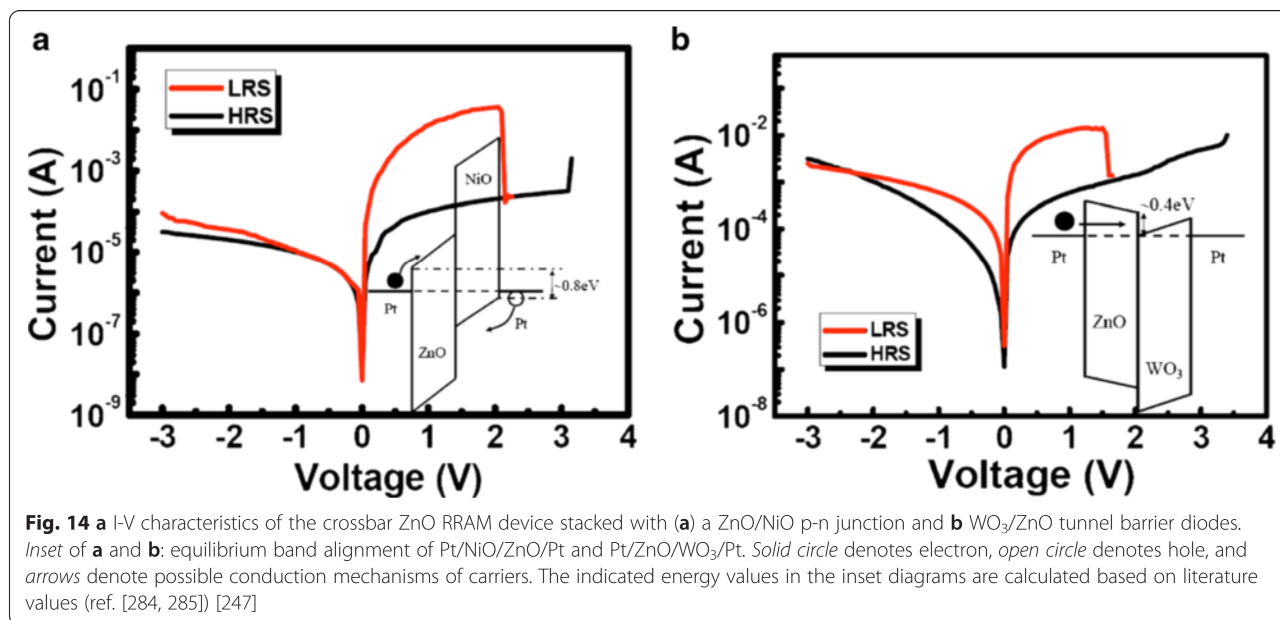

Fig. 14 **a** I-V characteristics of the crossbar ZnO RRAM device stacked with (**a**) a ZnO/NiO p-n junction and **b** WO_3/ZnO tunnel barrier diodes. *Inset* of **a** and **b**: equilibrium band alignment of Pt/NiO/ZnO/Pt and Pt/ZnO/WO_3/Pt. *Solid circle* denotes electron, *open circle* denotes hole, and *arrows* denote possible conduction mechanisms of carriers. The indicated energy values in the inset diagrams are calculated based on literature values (ref. [284, 285]) [247]

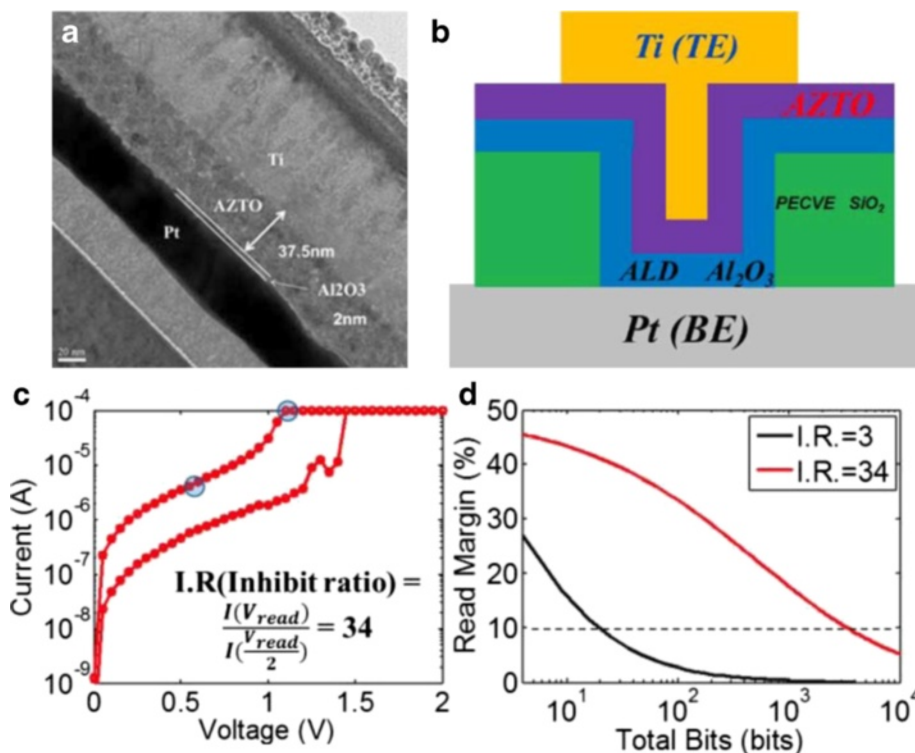

Fig. 15 a Cross-section TEM image of Ti/AZTO/Al_2O_3/Pt structure. **b** Schematic of the fabricated memory device structure. **c** Inhibit ratio (IR) of the nonlinear AZTO-based RRAM device. **d** The read margin analysis indicate that the proposed IR can extend array to ~3K bits [200]

vertically aligned nanorods may induce filament confinement, as depicted in Fig. 16c [256]. However, RRAM device made with ZnO nanorods layer with low packing density may suffer from short circuit problem due to direct contact between top and bottom electrodes [254]. Nevertheless, such issue can be avoided by embedding the nanorods layer in insulating polymers [253] or synthesizing highly densed nanorod film [216, 254]. In addition to that, employing nanorod layer may demonstrate surface self-cleaning function against water

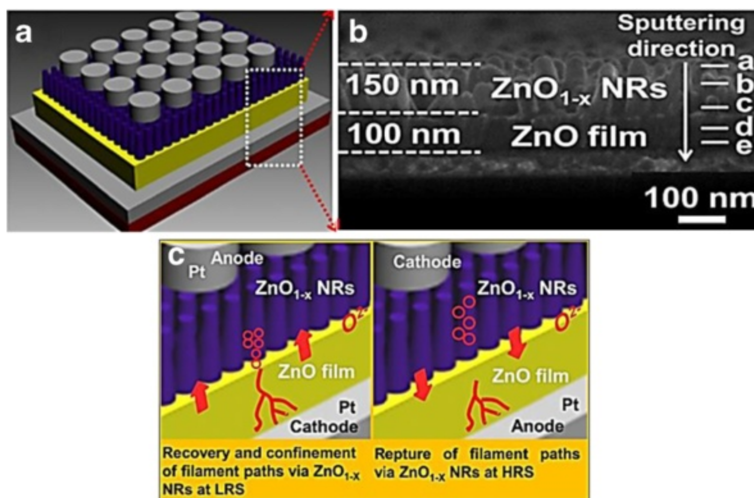

Fig. 16 a Schematic of a Pt/ZnO_{1-x} NRs/ZnO TF/Pt resistive switching device. **b** Corresponding SEM image of a well-aligned ZnO_{1-X} NR with a length of ~150 nm grown on the ZnO film with a thickness of ~100 nm. **c** Schematic of confined recovery and rupture of conducting filaments by ZnO_{1-x} NRs [256]

contact. Figure 17a, c shows hydrophilicity of ZnO thin film and hydrophobicity of ZnO nanorods, respectively [256]. Water-covered endurance characteristics of devices made with nanorod layer exhibit superior switching performance as compared to device without nanorods layer, shown in Fig. 17b, d, respectively [256]. This approach not only could avoid short circuit issue due to surface wetting but also could realize water resistant electronics. Moreover, memory performance of ZnO nanorods layer based devices can be further improved by embedding in higher concentration of polymethylmethacrylate [267] or surface hydrogen annealing [261].

Resistive memory employing laterally bridged ZnO nanorods, as shown in Fig. 18a, was developed in order to fabricate one-dimensional memory nanostructure that can meet mass production requirement [59]. Figure 18b demonstrates the peculiar unipolar switching [71] in a laterally bridged nanorod device in which the set voltage is smaller than the reset voltage that can prevent hard breakdown due to Joule heating during reset [59]. The formation and rupture of CF are situated at the nanorod/nanorod interfaces so that the actual memory cell size is incredibly smaller than the length of the nanorod itself.

Another effort to downsizing the physical dimension is by developing high scalability single nanorod/nanowire resistive device [60–75]. Orthogonal crossbar or vertically aligned nanorod/nanowire array RRAM devices could greatly increase storage density due to less substrate area consumption [61, 268]. Although such arrangement has not been reported yet due to its fabrication complexity, however, the development of these one-dimensional devices offers a novel understanding in resistive switching behavior on low-scale memory devices. Figure 19a, b shows SEM image and schematic of the Cu/Zn_2SnO_4-nanowire/Pd device structure, respectively [74]. Energy dispersive X-ray (EDX) analysis suggests that the Cu conductive bridge is formed in Cu/Zn_2SnO_4-nanowire/Pd device at the surface of nanorod, as depicted in Fig. 19c, d [74]. The evidence that metal atoms originated from active anode diffused under voltage bias, which the metal atoms are mainly distributed on the surface of the nanorod, is also reported in other ZnO-nanorod-based ECM type devices [70, 73]. Similarly, oxygen diffusion toward anode on the surface of a nanorod that leads to filament formation is also reported in ZnO-nanorod-based VCM type devices [69]. This confirmed earlier hypothesis that the formation of CF occurs on the surface/sidewall rather than within the bulk of the nanorod [252, 253].

Instability and reproducibility of resistive switching in single ZnO-nanorod/nanowire can be further improved by utilizing plasma treatment [60, 61] and introduction of other metal elements, such as Cu [66], Ga, and Sb [62]. It is also reported that self-compliance and self-rectifying characteristic can be induced by Na doping on ZnO-nanowire ECM type devices [70]. Single nanorod/nanowire-based devices offer ultra-low operation current, in the range of pico- to microamperes; however, the high operation voltage, in the range of hecto- to deka-volts, is still a main challenge in the development of this kind of resistive memory device [60–62, 66, 70, 75]. Despite ZnO:K,Cl micro/nanowire devices exhibited low operation voltage;

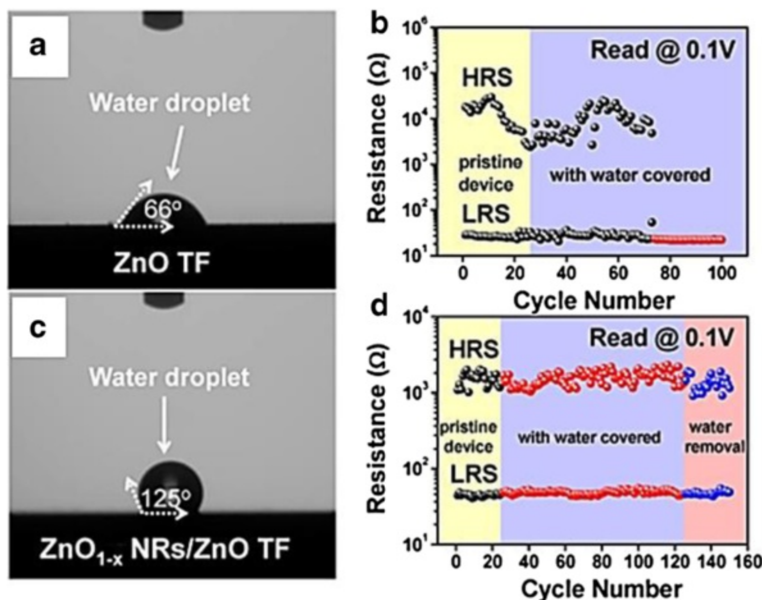

Fig. 17 **a**, **b** Contact angle measurements for surfaces of the ZnO film and the ZnO_{1-x} NRs, respectively. **c**, **d** Corresponding endurance tests for two devices measured with coverage of a water droplet at a read bias of 0.1 V, respectively [256]

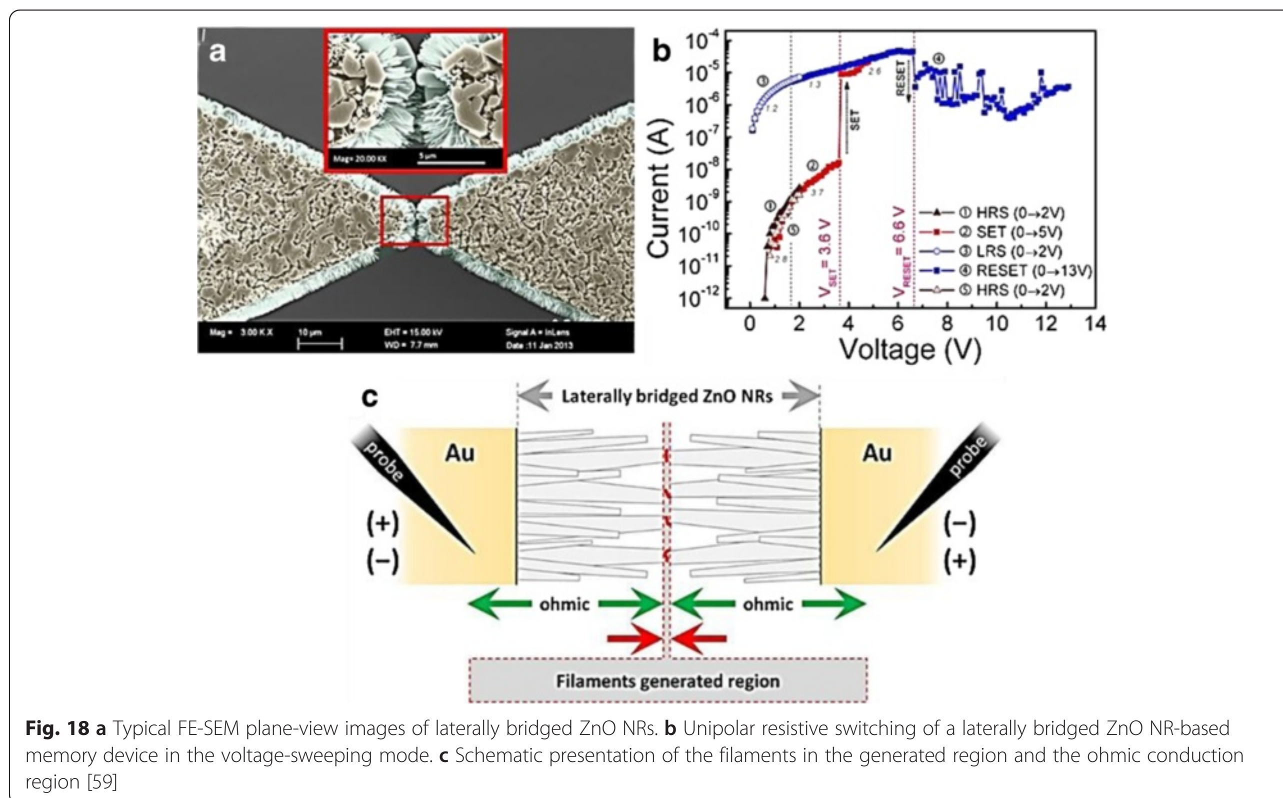

Fig. 18 a Typical FE-SEM plane-view images of laterally bridged ZnO NRs. **b** Unipolar resistive switching of a laterally bridged ZnO NR-based memory device in the voltage-sweeping mode. **c** Schematic presentation of the filaments in the generated region and the ohmic conduction region [59]

however, the operation current is in the range of milliamperes which is quite high for its class [63]. In another report, low current and voltage operation is exhibited in Ag/Zn_2SnO_3-sheated ZnO-core heterostructure nanowire/Ag device [67]; yet, the fabrication of this heterostructure is quite complex and may limit fabrication reproducibility.

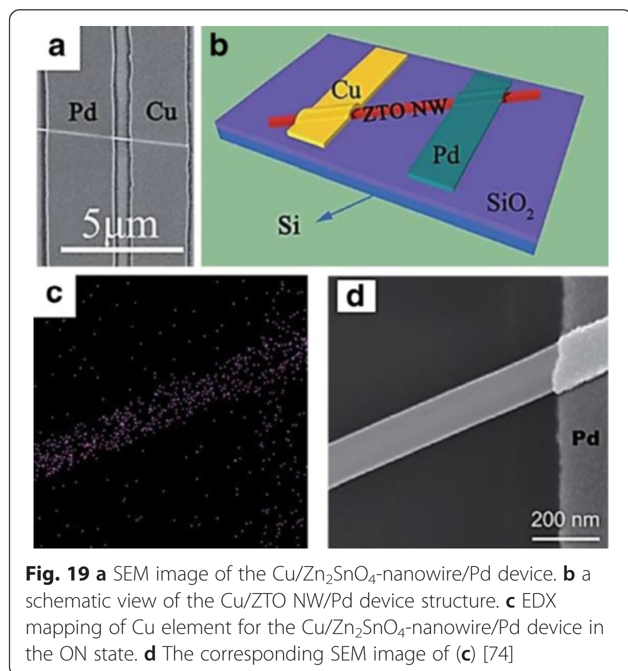

Fig. 19 a SEM image of the Cu/Zn_2SnO_4-nanowire/Pd device. **b** a schematic view of the Cu/ZTO NW/Pd device structure. **c** EDX mapping of Cu element for the Cu/Zn_2SnO_4-nanowire/Pd device in the ON state. **d** The corresponding SEM image of (**c**) [74]

In order to overcome the high operation voltage and current issue, the dimension of the switching device should be further scaled down. Figure 20a, b shows three-dimensional AFM and TEM images of single nanoisland grown by radio frequency plasma assisted SVTA ZnO MBE system on p^+-Si substrate [78]. The switching behavior of the single nanoisland devices was investigated by utilizing Cr/Co coated Si tip of conducting AFM (C-AFM) as a top electrode, as depicted in Fig. 20c [78]. The device shows counterclockwise bipolar characteristic, and the range of forming, set, and reset voltage is 5.4 to 9.7 V, 1.9 to 5 V, and −1 to −4.3 V, respectively [77]. Current compliance can be set as low as 10 μA, and higher memory window can be exhibited at further increase of current compliance to 500 μA, which indicate current compliance control multilevel characteristics observed in this device [77]. Interestingly, memory window increases as the diameter of the nanoisland decreases, followed by slightly increasing of HRS resistance, yet the LRS resistance exhibited independency to the diameter [77]. The C-AFM investigation during LRS shows that the highest current is distributed at the wall of the nanoisland, which once again confirmed that the CF prefers to occur at the surface of the nanostructure [69, 77]. It is found that current compliance also may control switching mode in a single nanoisland device [78]. Threshold-like and self-rectifying characteristics exhibited when current compliance was set at 10 and 100–10 μA, respectively, after forming process,

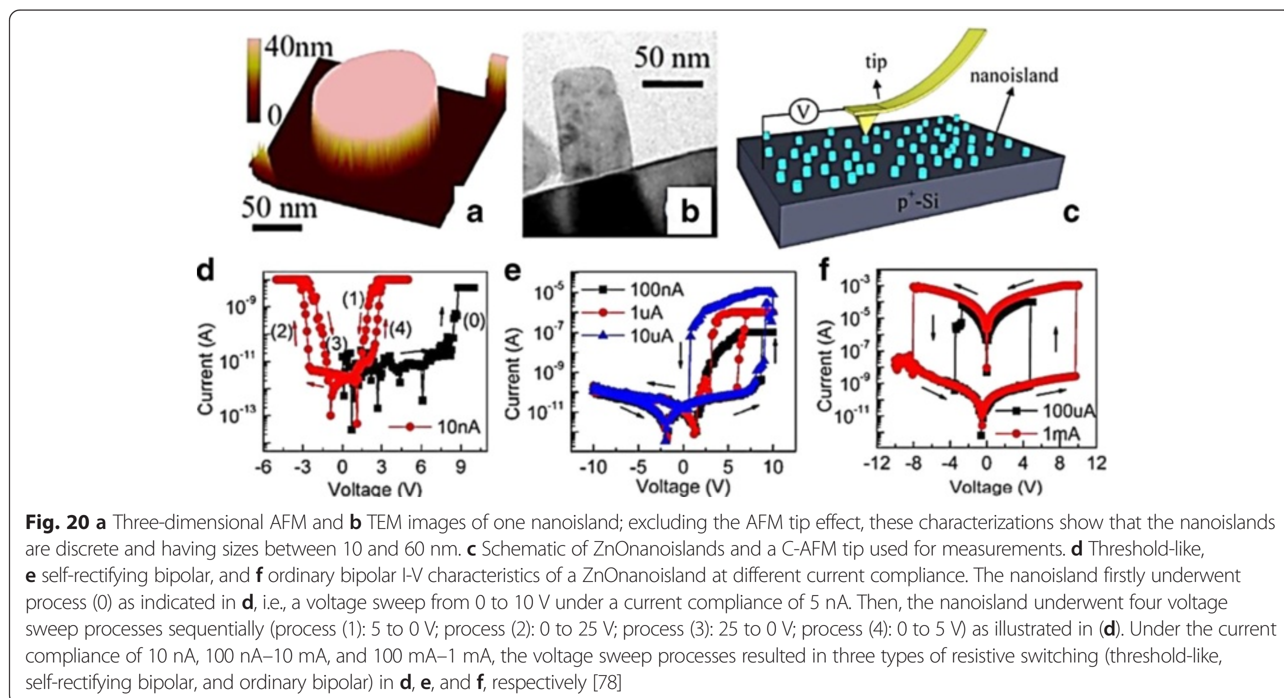

Fig. 20 a Three-dimensional AFM and **b** TEM images of one nanoisland; excluding the AFM tip effect, these characterizations show that the nanoislands are discrete and having sizes between 10 and 60 nm. **c** Schematic of ZnOnanoislands and a C-AFM tip used for measurements. **d** Threshold-like, **e** self-rectifying bipolar, and **f** ordinary bipolar I-V characteristics of a ZnOnanoisland at different current compliance. The nanoisland firstly underwent process (0) as indicated in **d**, i.e., a voltage sweep from 0 to 10 V under a current compliance of 5 nA. Then, the nanoisland underwent four voltage sweep processes sequentially (process (1): 5 to 0 V; process (2): 0 to 25 V; process (3): 25 to 0 V; process (4): 0 to 5 V) as illustrated in (**d**). Under the current compliance of 10 nA, 100 nA–10 mA, and 100 mA–1 mA, the voltage sweep processes resulted in three types of resistive switching (threshold-like, self-rectifying bipolar, and ordinary bipolar) in **d**, **e**, and **f**, respectively [78]

while higher than that ordinary bipolar was exhibited, as depicted in Fig. 20d–f [77, 78]. The ultra-low current compliance may control oxygen vacancies movement in the ZnO nanoisland, however, is not sufficient to form a CF [78]. Therefore, the occurrence of threshold-like and self-rectifying characteristics is due to the modulation of interfacial junction of top electrode/nanoisland and nanoisland/bottom electrode [78].

ZnO-Based RRAM as Multifunctional Devices

ZnO material offers a great potential in various electronic applications, such as photonic devices, spintronic devices, chemical and gas sensors, and transducers [81, 82]. It becomes more interesting when any of these properties can "coexist" with data storage applications in a single device. These multifunctional devices may revolutionize electronic circuitry, yet, still few progresses have been reported. In order to realize the multifunctional abilities, sufficient understanding in the relationship between one property and another is needed. Hence, stable and reliable multifunctional devices can be designed and fabricated appropriately.

For instance, ZnO-based transparent RRAM has a potential for being embedded in transparent wearable electronic gadget. In this case, the storage device is expected to have a stable operation in a real environment which may expose to various wavelength of light. Since ZnO is a light sensitive material that surface depletion region (SDR) may modulate the photo sensing ability; therefore, it is important to design a device that its light sensitivity should not or less affect to the resistive memory properties though it is also possible to design devices having both photonic and memory properties in the same time for certain applications.

Recent studies found that the ultra-violet (UV) irradiation may alter resistive switching property [58, 255, 258, 265, 269, 270]. Figure 21a–c shows the time-resolved photocurrent measurements at different resistance states in Pt/ZnO/Pt memory devices [269]. Initial resistance state (IRS) and high resistance state (HRS) exhibited photo response behavior under UV irradiation, while LRS is found independent to the UV light [269]. The pronounce photocurrent in IRS and HRS is due to the suppression of SDR that can be explained by these following equations:

$$O_{2(g)} + e^{-} \rightarrow O^{-}_{2(\mathrm{ad})} \quad (9)$$

$$O^{-}_{2(\mathrm{ad})} + h^{+} \rightarrow O_2 \quad (10)$$

where e^{-}, $O^{-}_{2(\mathrm{ad})}$, and h^{+} are single negatively charge electron, single negatively charge chemisorbed oxygen adatoms, and single positively charged hole. The chemisorbed oxygen adatoms in Eq. 9 induced SDR effect. When UV light with an energy higher than the ZnO band gap illuminates ZnO, electron-hole pairs are generated and Eq. 10 took place where the chemisorbed oxygen is discharged by photo-excited holes. The unpaired photo-excited electrons lead to photocurrent behavior in IRS and LRS; however, the metallic nature of the CF during LRS leads to independency to the light irradiation [269]. It is worth noted that the SDR need to

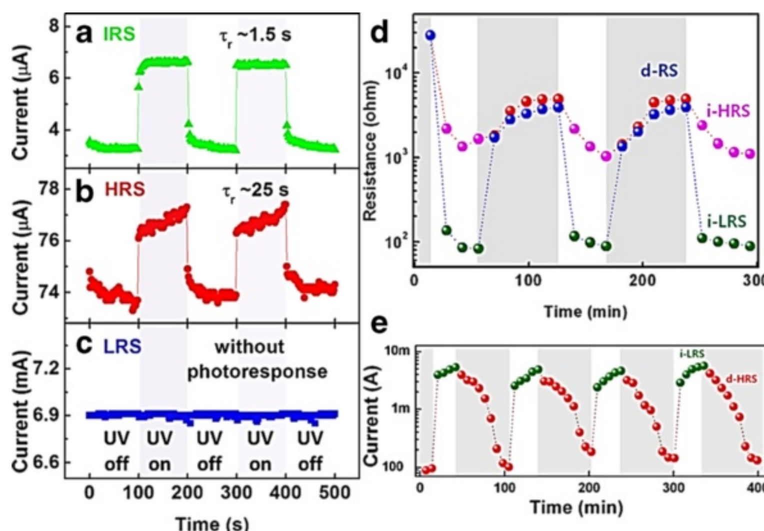

Fig. 21 Time-resolved photocurrent under 0.5 V bias of Pt/ZnO/Pt capacitors at UV wavelength of 365 nm in the (**a**) initial resistance state (IRS), **b** high-resistance state (HRS) and **c** low-resistance state (LRS) [269]. **d** RS characteristics of Au-coated ZnOnanorods/FTO memory devices were verified by repeating the sequence of SET and RESET processes; each data was extracted at 0.01 V and (**e**) with a time to current graph by repeating the sequence of d-HRS and i-LRS under alternating illumination (at a light wavelength of 200 to 2500 nm) and dark condition cycling [255]

be avoided or suppressed in ZnO-based RRAMs; it may introduce switching process instability [149, 217, 271, 272]. In addition to that, several studies suggested that resistive switching characteristics can be modulated using light irradiation treatment for several minutes [258, 270].

Interestingly, resistive switching characteristic dependent on constant light irradiation is also reported [58, 255, 265]. Figure 21d shows repetitive switching of Au-coated ZnO nanorods/FTO memory devices under dark and wide range of wavelength of light irradiation [255]. LRS and HRS can only be differentiated when the device is under irradiation. Similarly, the device can also be switched to HRS with photonic stimulus, as shown in Fig. 21e [255]. Excessive $O^{-}_{2(\mathrm{ad})}$ may easily recombine with oxygen vacancies regardless the applied voltage polarity, thus impeding CF formation under dark condition. Under light irradiation, the concentration of $O^{-}_{2(\mathrm{ad})}$ decreased due to photodesorption effect (Eq. 10) and makes CF formation possible. Good understanding in this unique relationship may allow us to expand and integrate memory and photonic application.

ZnO material, especially Co-doped ZnO, has also attracted great attention for room temperature-diluted magnetic semiconductor (DMS) applications [273–275]. Very recently, it is found that resistive switching characteristics have a direct correlation with magnetic modulation (MM) [139]. Figure 22a–f shows that resistive switching induced ferromagnetism in Pt/Co:ZnO/Pt devices [139]. The magnetic behavior can be easily tuned by simply changing the resistance state. The result in Fig. 22 shows that both saturation magnetization (Ms) and coercive field (Hc) are more pronounced in LRS [139]. This phenomenon can be explained using bound magnetic polarons (BMPs) model. Higher amount of oxygen vacancies created during LRS leads to higher volume occupied by BMPs; therefore, more Co^{2+} ions were overlapped into the ferromagnetic domains; conversely, the oxygen vacancy annihilation in HRS results in the decreasing of magnetic ordering, as presented in Fig. 22g–h [139]. Thus, this finding may encourage further development of multi-state data storage employing both electrical and magnetic properties.

Further exploration on the influence of light irradiation/exposure and magnetic modulation to the reliability and stability of switching characteristics are needed. Related to that, those reported studies only focus on VCM devices, while, based on our literature study, studies on multifunctional behavior on ECM devices are still less discussed. By employing the strain-induced polarization charges produced at the semiconductor/metal interface under externally applied deformation as a result of piezotronic effect, the switching characteristics of the CVD grown ZnO NW (diameter 500 nm; length 50 μm) resistive switching devices on PET are also reported [276]. In addition, the correlation between switching properties and other unique properties of ZnO such as lateral photovoltaic effect [277], electroluminescence [278, 279], piezoelectricity [276, 280, 281], light emitters [282] are still not yet fully explored.

Apart from its potential as a multifunctional RRAM material, ZnO performance among other oxides-based is also quite comparative. Table 6 shows performance comparison between different metal oxides in published literature. ZnO may offer sufficient endurance and memory window

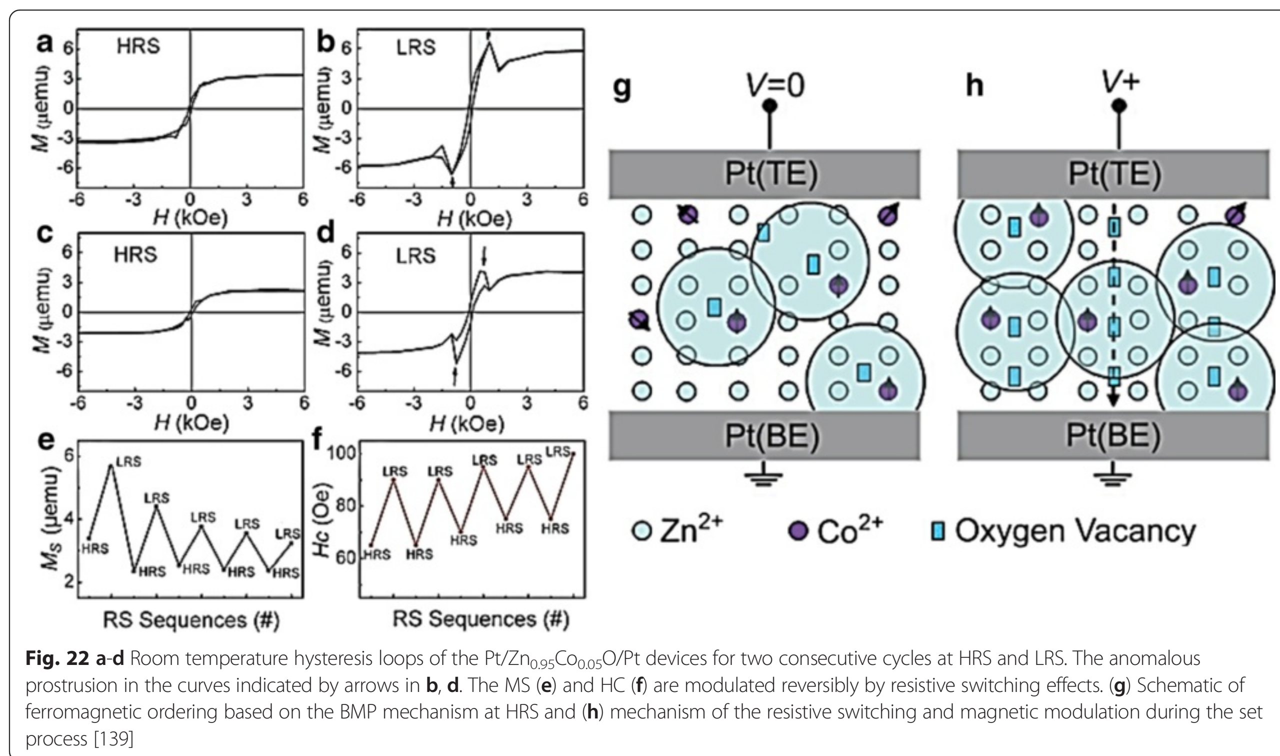

Fig. 22 a-d Room temperature hysteresis loops of the Pt/$Zn_{0.95}Co_{0.05}O$/Pt devices for two consecutive cycles at HRS and LRS. The anomalous prostrusion in the curves indicated by arrows in **b**, **d**. The MS (**e**) and HC (**f**) are modulated reversibly by resistive switching effects. (**g**) Schematic of ferromagnetic ordering based on the BMP mechanism at HRS and (**h**) mechanism of the resistive switching and magnetic modulation during the set process [139]

with acceptable retention performance; yet, much lower operation current and faster operation speed using other oxides are reported. This indicates that low current operation and tolerable operation speed are a great challenge for the development of ZnO-based RRAM. In addition, the development of ultra-thin ZnO-based RRAM is needed, since utilization of switching layer is expected to scale down to 1× nm in the near future [283].

Conclusions

In the case of VCM cell, the area of switching region can be controlled by modulating the microstructural properties and defects concentration of ZnO films; however, in ECM cell, relying only on those factors are insufficient; another technique, probably by electrode engineering approach, needs to be developed in order to control the Joule heating effective region.

Table 6 Performance comparison of Pt or Ag/metal oxide/Pt in published literature

No	Structure	SL thickness (nm)	Maximum operation current (mA)	Set/reset operation speed (μs)	Endurance/ratio (cycles)/(times)	Retention (seconds or hours)	Stress (seconds)	Ref.
1	Pt/ZnO/Pt	25	3	10^4	10^6(AC)/>10^2	>6 × 10^5s/RT	NA	[122]
2	Pt/Al_2O_3/Pt	2	~1	0.07	$10^5/10^2$	NA	NA	[289]
3	Pt/NiO/Pt	10	0.1	0.1/~1	100/~10	1000 h/150 °C	NA	[290]
4	Pt/TaOx/Pt	30	<0.17	0.01	10^9/~10	3000 h/150 °C	NA	[291]
5	Pt/TiO_2/Pt	27	3	DC	80/~10^2	NA	NA	[292]
6	Pt/ZrO_2/Pt	130	~10	10^4/5 × 10^4	$10^5/10^3$	NA	NA	[293]
7	Pt/Gd_2O_3/Pt	120	35	DC	60/>10^6	30 h/85 °C	NA	[294]
8	Ag/ZnO/Pt	100	10	DC	40/10^2	NA	10^4/RT	[124]
9	Ag/La_2O_3/Pt	50	0.035	DC	>10^3/>10^3	10^6 s/RT	NA	[295]
10	Ag/SiO_2/Pt	80	0.5	DC	~35/10^6	~2 × 10^3s/RT	NA	[296]
11	Ag/TaO_x/Pt	65	~100	NA	NA	NA	NA	[297]
12	Ag/ZrO_2/Pt	50	5	DC	>10^2/>10^2	NA	~7.5 × 10^3/RT	[298]
13	Ag/TiO_2/Pt	40	0.29	100/10^3	~10/~10^6	10^4 s/RT	NA	[299]

RT measured at room temperature, *NA* data not available, *DC* direct-current voltage sweeping mode

Both VCM and ECM cells require high resistivity of ZnO films in order to achieve suitable memory effect. Though several efforts have been conducted to suppress the native defects concentration to achieve less leakage current, yet development of p-type and superoxide ZnO-based RRAM has not been explored yet. The development of highly resistive ZnO film may open the possibility to thinning down the switching layer and lowering the current operation; fabrication of ultra-thin and low power device is the major challenge in this oxide system. ZnO nanoisland-based switching memory device is a promising approach for the low power scalable memory devices.

It is also quite interesting and challenging at the same time to explore the multifunctional RRAM. Up to now, most reports on these correlation studies are still only in the early stage. We believe that investigation and development of multifunctional nonvolatile memory devices will attract significant interest in the near future.

Acknowledgements
This work was supported by the Ministry of Science and Technology, Taiwan, under project NSC 102-2221-E009-134-MY3.

Authors' contributions
FMS collected and reviewed the references and wrote the first draft. DP wrote 'sneak current prevention in ZnO-based RRAM' section. The final draft was modified by DP, TYT. The final manuscript checked by KHW. All authors read and approved the final manuscript.

Authors' information
FMS received his BE degree in Materials and Metallurgy Engineering from Sepuluh Nopember Institute of Technology (ITS), Indonesia and MS degree in Mechanical Engineering from National Taiwan University of Science and Technology (NTUST), Taiwan. He is currently a Ph.D. candidate of Materials Science and Engineering Department of National Chiao Tung University (NCTU), Taiwan. He is working at Electronic Materials Laboratory of Electronics Engineering Department of NCTU where he responsible for the development of ZnO-based transparent resistive random access memory devices, under the supervision of TYT. He specializes in surface and interfaces analysis, solid-state materials characterization, synthesis of nanostructured materials and device fabrication. He received a number of awards and scholarships, such as NCTU Outstanding Students Award, MME-ITS Mawapres Award and IEFE Dissertation Scholarships.
DP completed his Ph.D. from Indian Institute of Technology Kharagpur, India. After that, he joined as a post-doctoral fellow at Department of Electronics and Communication Engg., National Chiao Tung University, Taiwan, and Department of Electrical and Computer Engg., University of Utah, USA. Prior to joining in the department of Physics and Electronics Eng., National Institute of Science and Technology, Berhampur, India, as an associate professor he also served as a post-doctoral fellow at the Department of Electrical and Computer Engg., National University of Singapore, Singapore. At present he serving as head of the department of Physics at National Institute of Science and Technology, Berhampur, India. Recently, he is awarded summer research fellowship 2016 by three Indian academies. His present research interest includes the design and fabrication of low power, high reliable transparent non-volatile memory devices at low process temperature. he is serving as a reviewer for a number of international journals including, IEEE, AIP, IOP, RSC, ACS, Elsevier, etc. and also a reviewer of international European project council. DP published more than 23 international refereed journal papers and 40 international conference proceedings; several review articles and a book chapter in his credit. He is a fellow of Indian Physical Society
KHW is a Chair Professor in the Department of Materials Science and Engineering, National Chiao Tung University (NCTU). He is the Dean of the College of Engineering in NCTU. He received numerous awards, such as the Outstanding Research Award from the Ministry of Science and Technology, Taiwan (2003, 2010, 2014), material science award such as Ho Chin Tui Award (2014) and is a Fellow, of Materials Research Society, Taiwan (2011). He has published more than 180 peer-reviewed SCI journal papers with more 10,000 citations.
TYT is now a Lifetime Chair Professor in the Department of Electronics Engineering, National Chiao Tung University. He was the Dean of the College of Engineering and Vice Chancellor of the National Taipei University of Technology. He received numerous awards, such as the Distinguished Research Award from the National Science Council, Academic Award of the Ministry of Education, National Endowed Chair Professor, and IEEE CPMT Outstanding Sustained Technical Contribution Award. He is a Fellow of IEEE and American Ceramic Society.

Competing Interests
The authors declare that they have no competing interests.

Author details
[1]Department of Materials Science and Engineering, National Chiao Tung University, Hsinchu 30010, Taiwan. [2]Department of Electronics Engineering, National Institute of Science and Technology, Berhampur, Odisha 761008, India. [3]Department of Electronics Engineering and Institute of Electronics, National Chiao Tung University, Hsinchu 30010, Taiwan.

Received: 12 June 2016 Accepted: 3 August 2016
Published online: 19 August 2016

References

1. Bez R, Camerlenghi E, Modelli A, Visconti A (2003) Introduction to flash memory. Proc IEEE 91:489–502. doi:10.1109/JPROC.2003.811702
2. Tseng T-Y, Sze SM (2012) Nonvolatile memories materials, devices and applications, Vol. 1. American Scientific Publishers, CA. USA. ISBN:1-58883-250-3
3. Panda D, Panda M (2016) Non-volatile flash memory characteristics of tetralayer nickel-germanide nanocrystals embedded structure. J Nanosci Nanotechnol 16:1216–1219. doi:10.1166/jnn.2016.11047
4. Panda D, Dhar A, Ray SK (2009) Improved charge storage characteristics of the tetralayer non-volatile memory structure using nickel nanocrystal trapping layer. Semicond Sci Technol 24:115020. doi:10.1088/0268-1242/24/11/115020
5. Panda D, Maikap S, Dhar a, Ray SK (2009) Memory characteristics of nickel nanocrystals with high-k dielectric tunneling barriers. Electrochem Solid-State Lett 12:H7. doi:10.1149/1.3006024
6. Makarov a, Sverdlov V, Selberherr S (2012) Emerging memory technologies: trends, challenges, and modeling methods. Microelectron Reliab 52:628–634. doi:10.1016/j.microrel.2011.10.020
7. Seo Y, Song MY, An H, Kim TG (2013) A CMOS-process-compatible ZnO-based charge-trap flash memory. IEEE Electron Device Lett 34:238–240. doi:10.1109/LED.2012.2235059
8. El-Atab N, Cimen F, Alkis S, Okyay AK, Nayfeh A (2014) Enhanced memory effect with embedded graphene nanoplatelets in ZnO charge trapping layer. Appl Phys Lett 105:033102. doi:10.1063/1.4891050
9. He S, Bai H, Liu G, Li Q, Yan S, Chen Y, Mei L, Liu H, Wang S, Han X (2012) Enhanced tunnel magnetoresistance in fully epitaxial ZnO:Co-based magnetic tunnel junctions with Mg-doped ZnO barrier. Appl Phys Lett 100: 132406. doi:10.1063/1.3698151
10. Yeh M-S, Wu Y-C, Hung M-F, Liu K-C, Jhan Y-R, Chen L-C, Chang C-Y (2013) Fabrication, characterization and simulation of Ω-gate twin poly-Si FinFET nonvolatile memory. Nanoscale Res Lett 8:331. doi:10.1186/1556-276X-8-331
11. Avrutin V, Izyumskaya N, Ozgur U, Silversmith DJ, Morkoç H (2010) Ferromagnetism in ZnO- and GaN-based diluted magnetic semiconductors: achievements and challenges. Proc IEEE 98:1288–1301. doi:10.1109/JPROC.2010.2044966
12. Bak JY, Yoon SM (2014) High-performance transparent, all-oxide nonvolatile charge trap memory transistor using In-Ga-Zn-O channel and ZnO trap layer. J Vac Sci Technol 32:060604. doi:10.1116/1.4899180
13. Lee YT, Ali Raza SR, Jeon PJ, Ha R, Choi H-J, Im S (2013) Long single ZnO nanowire for logic and memory circuits: NOT, NAND, NOR gate, and SRAM. Nanoscale 5:4181–5. doi:10.1039/c3nr01015e

14. Jia Z, Zhang M-M, Ren T-L (2011) Modulation effect of lead zirconate titanate for zinc oxide channel resistance in ferroelectric field effect transistor. Ferroelectrics 421:92–97. doi:10.1080/00150193.2011.594734
15. Gupta D, Anand M, Ryu SW, Choi YK, Yoo S (2008) Nonvolatile memory based on sol-gel ZnO thin-film transistors with Ag nanoparticles embedded in the ZnO/gate insulator interface. Appl Phys Lett 93:1–4. doi:10.1063/1.3041777
16. Yoon J, Hong W-K, Jo M, Jo G, Choe M, Park W, Sohn JI, Nedic S, Hwang H, Welland ME, Lee T (2011) Nonvolatile memory functionality of ZnO nanowire transistors controlled by mobile protons. ACS Nano 5:558–564. doi:10.1021/nn102633z
17. Cha SH, Park A, Lee KH, Im S, Lee BH, Sung MM (2010) Pentacene thin-film on organic/inorganic nanohybrid dielectrics for ZnO charge injection memory transistor. Org Electron 11:159–163. doi:10.1016/j.orgel.2009.09.021
18. Switzer JA, Gudavarthy RV, Kulp EA, Mu G, He Z, Wessel AJ (2010) Resistance switching in electrodeposited magnetite superlattices. J Am Chem Soc 132:1258–1260. doi:10.1021/ja909295y
19. Wang G, Chen Y, Shen X, Li J, Wang R, Lu Y, Dai S, Xu T, Nie Q (2014) Reversibility and stability of ZnO-Sb 2 Te 3 nanocomposite films for phase change memory applications. ACS Appl Mater Interfaces 6:8488–8496. doi:10.1021/am501345x
20. Comesaña E, Aldegunde M, García-Loureiro a J, Gehring G a (2010) Simulation of the tunnelling transport in ferromagnetic GaAs/ZnO heterojunctions. J Phys Conf Ser 242:012015. doi:10.1088/1742-6596/242/1/012015
21. Kim E, Kim Y, Han Kim D, Lee K, Parsons GN, Park K (2011) SiNx charge-trap nonvolatile memory based on ZnO thin-film transistors. Appl Phys Lett 99:11–14. doi:10.1063/1.3640221
22. Li Q, Shen T-T, Cao Y-L, Zhang K, Yan S-S, Tian Y-F, Kang S-S, Zhao M-W, Dai Y-Y, Chen Y-X, Liu G-L, Mei L-M, Wang X-L, Grünberg P (2014) Spin memristive magnetic tunnel junctions with CoO-ZnO nano composite barrier. Sci Rep 4:3835. doi:10.1038/srep03835
23. Oruc FB, Cimen F, Rizk A, Ghaffari M, Nayfeh A, Okyay AK (2012) Thin-film ZnO charge-trapping memory cell grown in a single ALD step. IEEE Electron Device Lett 33:1714–1716. doi:10.1109/LED.2012.2219493
24. Park CH, Im S, Yun J, Lee GH, Lee BH, Sung MM (2009) Transparent photostable ZnO nonvolatile memory transistor with ferroelectric polymer and sputter-deposited oxide gate. Appl Phys Lett 95:223506. doi:10.1063/1.3269576
25. Tsymbal EY (2006) Applied physics: tunneling across a ferroelectric. Science (80-) 313:181–183. doi:10.1126/science.1126230
26. Kahng D, Sze SM (1967) A floating gate and its application to memory devices. Bell Syst Tech J 46:1288–1295. doi:10.1002/j.1538-7305.1967.tb01738.x
27. Terabe K, Hasegawa T, Nakayama T, Aono M (2005) Quantized conductance atomic switch. Nature 433:47–50. doi:10.1038/nature03190
28. Cen C, Thiel S, Mannhart J, Levy J (2009) Oxide nanoelectronics on demand. Science 323:1026–1030. doi:10.1126/science.1168294
29. Wuttig M, Yamada N (2007) Phase-change materials for rewriteable data storage. Nat Mater 6:824–832. doi:10.1038/nmat2009
30. Panda D, Dhar A, Ray SK (2008) Schottky barrier characteristics of cobalt-nickel silicide/n-Si junctions for scaled-Si CMOS applications. IEEE Trans Electron Devices 55:2403–2408. doi:10.1109/TED.2008.927632
31. Waser R, Aono M (2007) Nanoionics-based resistive switching memories. Nat Mater 6:833–40. doi:10.1038/nmat2023
32. Strukov DB, Snider GS, Stewart DR, Williams RS (2008) The missing memristor found. Nature 453:80–3. doi:10.1038/nature06932
33. Panda D, Tseng T-Y (2013) Growth, dielectric properties, and memory device applications of ZrO2 thin films. Thin Solid Films 531:1–20. doi:10.1016/j.tsf.2013.01.004
34. Panda D, Tseng T-Y (2014) Perovskite oxides as resistive switching memories: a review. Ferroelectrics 471:23–64. doi:10.1080/00150193.2014.922389
35. Li Y, Long S, Liu Q, Lü H, Liu S, Liu M (2011) An overview of resistive random access memory devices. Chinese Sci Bull 56:3072–3078. doi:10.1007/s11434-011-4671-0
36. Lin C-Y, Liu C-Y, Lin C-C, Tseng TY (2007) Current status of resistive nonvolatile memories. J Electroceramics 21:61–66. doi:10.1007/s10832-007-9081-y
37. Jeong DS, Thomas R, Katiyar RS, Scott JF, Kohlstedt H, Petraru a, Hwang CS (2012) Emerging memories: resistive switching mechanisms and current status. Rep Prog Phys 75:076502. doi:10.1088/0034-4885/75/7/076502
38. Lee J, Jo M, Seong D, Shin J, Hwang H (2011) Materials and process aspect of cross-point RRAM (invited). Microelectron Eng 88:1113–1118. doi:10.1016/j.mee.2011.03.035
39. Yang JJ, Pickett MD, Li X, Ohlberg D a a, Stewart DR, Williams RS (2008) Memristive switching mechanism for metal/oxide/metal nanodevices. Nat Nanotechnol 3:429–33. doi:10.1038/nnano.2008.160
40. Yang JJ, Inoue IH, Mikolajick T, Hwang CS (2012) Metal oxide memories based on thermochemical and valence change mechanisms. MRS Bull 37:131–137. doi:10.1557/mrs.2011.356
41. Yang Y, Lu W (2013) Nanoscale resistive switching devices: mechanisms and modeling. Nanoscale 5:10076–92. doi:10.1039/c3nr03472k
42. Pan F, Chen C, Wang Z, Yang Y, Yang J, Zeng F (2010) Nonvolatile resistive switching memories-characteristics, mechanisms and challenges. Prog Nat Sci Mater Int 20:1–15. doi:10.1016/S1002-0071(12)60001-X
43. Pan F, Gao S, Chen C, Song C, Zeng F (2014) Recent progress in resistive random access memories: materials, switching mechanisms, and performance. Mater Sci Eng R Reports 83:1–59. doi:10.1016/j.mser.2014.06.002
44. Waser R, Dittmann R, Staikov G, Szot K (2009) Redox-based resistive switching memories—nanoionic mechanisms, prospects, and challenges. Adv Mater 21:2632–2663. doi:10.1002/adma.200900375
45. Akinaga H, Shima H (2010) Resistive random access memory (ReRAM) based on metal oxides. Proc IEEE 98:2237–2251. doi:10.1109/JPROC.2010.2070830
46. Zhu X-J, Shang J, Li R-W (2012) Resistive switching effects in oxide sandwiched structures. Front Mater Sci 6:183–206. doi:10.1007/s11706-012-0170-8
47. Chua L. Memristor-The missing circuit element. IEEE Trans Circuit Theory. doi: 10.1109/TCT.1971.1083337
48. Tour JM, He T (2008) Electronics: the fourth element. Nature 453:42–43. doi:10.1038/453042a
49. Hickmott TW (1962) Low-frequency negative resistance in thin anodic oxide films. J Appl Phys 33:2669. doi:10.1063/1.1702530
50. Gibbons JF, Beadle WE (1964) Switching properties of thin NiO films. Solid State Electronics 7:785–90. doi:10.1016/0038-1101(64)90131-5
51. Simmons JG, Verderber RR (1967) New conduction and reversible memory phenomena in thin insulating films. Proc R Soc A Math Phys Eng Sci 301:77–102. doi:10.1098/rspa.1967.0191
52. Huang H-W, Kang C-F, Lai F-I, He J-H, Lin S-J, Chueh Y-L (2013) Stability scheme of ZnO-thin film resistive switching memory: influence of defects by controllable oxygen pressure ratio. Nanoscale Res Lett 8:483. doi:10.1186/1556-276X-8-483
53. Wang ZQ, Xu HY, Zhang L, Li XH, Ma JG, Zhang XT, Liu YC (2013) Performance improvement of resistive switching memory achieved by enhancing local-electric-field near electromigrated Ag-nanoclusters. Nanoscale 5:4490–4. doi:10.1039/c3nr33692a
54. Simanjuntak FM, Panda D, Tsai T-L, Lin C-A, Wei K-H, Tseng T-Y (2015) Enhanced switching uniformity in AZO/ZnO1−x/ITO transparent resistive memory devices by bipolar double forming. Appl Phys Lett 107:033505. doi:10.1063/1.4927284
55. Chen X, Hu W, Wu S, Bao D (2014) Stabilizing resistive switching performances of TiN/MgZnO/ZnO/Pt heterostructure memory devices by programming the proper compliance current. Appl Phys Lett 104:043508. doi:10.1063/1.4863744
56. Zhuge F, Peng S, He C, Zhu X, Chen X, Liu Y, Li R-W (2011) Improvement of resistive switching in Cu/ZnO/Pt sandwiches by weakening the randomicity of the formation/rupture of Cu filaments. Nanotechnology 22:275204. doi:10.1088/0957-4484/22/27/275204
57. Shih A, Zhou W, Qiu J, Yang H-J, Chen S, Mi Z, Shih I (2010) Highly stable resistive switching on monocrystalline ZnO. Nanotechnology 21:125201. doi:10.1088/0957-4484/21/12/125201
58. Kathalingam A, Kim HS, Kim SD, Park HC (2015) Light induced resistive switching property of solution synthesized ZnO nanorod. Opt Mater (Amst) 48:190–197. doi:10.1016/j.optmat.2015.08.001
59. Chuang M-Y, Chen Y-C, Su Y-K, Hsiao C-H, Huang C-S, Tsai J-J, Yu H-C (2014) Negative differential resistance behavior and memory effect in laterally bridged ZnO nanorods grown by hydrothermal method. ACS Appl Mater Interfaces 6:5432–8. doi:10.1021/am404875s
60. Lai Y, Qiu W, Zeng Z, Cheng S, Yu J, Zheng Q (2016) Resistive switching of plasma-treated zinc oxide nanowires for resistive random access memory. Nanomaterials 6:16. doi:10.3390/nano6010016
61. Lai Y, Xin P, Cheng S, Yu J, Zheng Q (2015) Plasma enhanced multistate storage capability of single ZnO nanowire based memory. Appl Phys Lett 106:031603. doi:10.1063/1.4906416
62. Wang B, Ren T, Chen S, Zhang B, Zhang R, Qi J, Chu S, Huang J, Liu J (2015) Resistive switching in Ga- and Sb-doped ZnO single nanowire devices. J Mater Chem C 3:11881–11885. doi:10.1039/C5TC02102B

63. Zhao J, Cheng B, Xiao Y, Guo R, Lei S (2015) Ultrahigh performance negative thermal-resistance switching based on individual ZnO:K, Cl micro/nanowires for multibit nonvolatile resistance random access memory dual-written/erased repeatedly by temperature or bias. J Mater Chem C 3:12220–12229. doi:10.1039/C5TC02824H
64. Huang C-W, Chen J-Y, Chiu C-H, Wu W-W (2014) Revealing controllable nanowire transformation through cationic exchange for RRAM application. Nano Lett 14:2759–63. doi:10.1021/nl500749q
65. Huang Y, Luo Y, Shen Z, Yuan G, Zeng H (2014) Unipolar resistive switching of ZnO-single-wire memristors. Nanoscale Res Lett Springer :1-5. doi: 10.1186/1556-276X-9-381
66. Lai Y, Wang Y, Cheng S, Yu J (2014) Defects and resistive switching of zinc oxide nanorods with copper addition grown by hydrothermal method. J Electron Mater 43:2676–2682. doi:10.1007/s11664-014-3116-3
67. Cheng B, Ouyang Z, Chen C, Xiao Y, Lei S (2013) Individual Zn2SnO4-sheathed ZnO heterostructure nanowires for efficient resistive switching memory controlled by interface states. Sci Rep 3:3249. doi:10.1038/srep03249
68. Dugaiczyk L, Ngo-Duc T-T, Gacusan J, Singh K, Yang J, Santhanam S, Han J-W, Koehne JE, Kobayashi NP, Meyyappan M, Oye MM (2013) Resistive switching in single vertically-aligned ZnO nanowire grown directly on Cu substrate. Chem Phys Lett 575:112–114. doi:10.1016/j.cplett.2013.05.005
69. Huang Y-T, Yu S-Y, Hsin C-L, Huang C-W, Kang C-F, Chu F-H, Chen J-Y, Hu J-C, Chen L-T, He J-H, Wu W-W (2013) In situ TEM and energy dispersion spectrometer analysis of chemical composition change in ZnO nanowire resistive memories. Anal Chem 85:3955–60. doi:10.1021/ac303528m
70. Qi J, Huang J, Paul D, Ren J, Chu S, Liu J (2013) Current self-complianced and self-rectifying resistive switching in Ag-electroded single Na-doped ZnO nanowires. Nanoscale 5:2651–4. doi:10.1039/c3nr00027c
71. Chiang Y, Chang W, Ho C, Chen C, Ho C (2011) Single-ZnO-nanowire memory. IEEE Trans Electron Devices 58:1735–1740. doi:10.1109/TED.2011.2121914
72. Mohan R, Kim SJ (2011) Current biased resistive switching in ZnO whiskers. Jpn J Appl Phys 50:1–5. doi:10.1143/JJAP.50.04DJ01
73. Yang Y, Zhang X, Gao M, Zeng F, Zhou W, Xie S, Pan F (2011) Nonvolatile resistive switching in single crystalline ZnO nanowires. Nanoscale 3:1917–21. doi:10.1039/c1nr10096c
74. Dong H, Zhang X, Zhao D, Niu Z, Zeng Q, Li J, Cai L, Wang Y, Zhou W, Gao M, Xie S (2012) High performance bipolar resistive switching memory devices based on Zn2SnO4 nanowires. Nanoscale 4:2571–4. doi:10.1039/c2nr30133d
75. Lin DD, Wu H, Pan W (2007) Photoswitches and memories assembled by electrospinning aluminum-doped zinc oxide single nanowires. Adv Mater 19:3968–3972. doi:10.1002/adma.200602802
76. Yang Y, Qi J, Guo W, Qin Z, Zhang Y (2010) Electrical bistability and negative differential resistance in single Sb-doped ZnO nanobelts/SiOx/p-Si heterostructured devices. Appl Phys Lett 96:2008–2011. doi:10.1063/1.3339873
77. Qi J, Olmedo M, Ren J, Zhan N, Zhao J, Zheng J, Liu J (2012) Resistive switching in single epitaxial ZnO nanoislands. ACS Nano 6:1051–1058. doi:10.1021/nn204809a
78. Qi J, Olmedo M, Zheng J-G, Liu J (2013) Multimode resistive switching in single ZnO nanoisland system. Sci Rep 3:2405. doi:10.1038/srep02405
79. Cho B, Song S, Ji Y, Kim TW, Lee T (2011) Organic resistive memory devices: performance enhancement, integration, and advanced architectures. Adv Funct Mater 21:2806–2829. doi:10.1002/adfm.201100686
80. Yoo EJ, Lyu M, Yun J-H, Kang CJ, Choi YJ, Wang L (2015) Resistive Switching Behavior in Organic-Inorganic Hybrid $CH_3NH_3PbI_{3-x}Cl_x$ Perovskite for Resistive Random Access Memory Devices. Adv Mater :n/a–n/a. doi: 10.1002/adma.201502889
81. Djurisić AB, Leung YH (2006) Optical properties of ZnO nanostructures. Small 2:944–961. doi:10.1002/smll.200600134
82. Panda D, Tseng T-Y (2013) One-dimensional ZnO nanostructures: fabrication, optoelectronic properties, and device applications. J Mater Sci 48:6849–6877. doi:10.1007/s10853-013-7541-0
83. Xu Z, Yu L, Xu X, Miao J, Jiang Y (2014) Effect of oxide/oxide interface on polarity dependent resistive switching behavior in ZnO/ZrO2 heterostructures. Appl Phys Lett 104:192903. doi:10.1063/1.4878402
84. Huang C-H, Huang J-S, Lai C-C, Huang H-W, Lin S-J, Chueh Y-L (2013) Manipulated transformation of filamentary and homogeneous resistive switching on ZnO thin film memristor with controllable multistate. ACS Appl Mater Interfaces 5:6017–23. doi:10.1021/am4007287
85. Xu D, Xiong Y, Tang M, Zeng B (2014) Coexistence of the bipolar and unipolar resistive switching behaviors in vanadium doped ZnO films. J Alloys Compd 584:269–272. doi:10.1016/j.jallcom.2013.09.073
86. Xu DL, Xiong Y, Tang MH, Zeng BW, Xiao YG (2014) Bipolar and unipolar resistive switching modes in Pt/Zn0.99Zr0.01O/Pt structure for multi-bit resistance random access memory. Appl Phys Lett 104:183501. doi:10.1063/1.4875383
87. Xu Q, Wen Z, Wu D (2011) Bipolar and unipolar resistive switching in Zn 0.98 Cu 0.02 O films. J Phys D Appl Phys 44:335104. doi:10.1088/0022-3727/44/33/335104
88. Lee S, Kim H, Park J, Yong K (2010) Coexistence of unipolar and bipolar resistive switching characteristics in ZnO thin films. J Appl Phys 108:2008–2011. doi:10.1063/1.3489882
89. Chen J-Y, Hsin C-L, Huang C-W, Chiu C-H, Huang Y-T, Lin S-J, Wu W-W, Chen L-J (2013) Dynamic evolution of conducting nanofilament in resistive switching memories. Nano Lett 13:3671–3677. doi:10.1021/nl4015638
90. Murali S, Rajachidambaram JS, Han S-Y, Chang C-H, Herman GS, Conley JF (2013) Resistive switching in zinc–tin-oxide. Solid State Electron 79:248–252. doi:10.1016/j.sse.2012.06.016
91. Peng HY, Li GP, Ye JY, Wei ZP, Zhang Z, Wang DD, Xing GZ, Wu T (2010) Electrode dependence of resistive switching in Mn-doped ZnO: filamentary versus interfacial mechanisms. Appl Phys Lett 96:192113. doi:10.1063/1.3428365
92. Hsu CH, Fan YS, Liu PT (2013) Multilevel resistive switching memory with amorphous InGaZnO-based thin film. Appl Phys Lett 102:2013–2016. doi:10.1063/1.4792316
93. Yang Y, Gao P, Gaba S, Chang T, Pan X, Lu W (2012) Observation of conducting filament growth in nanoscale resistive memories. Nat Commun 3:732. doi:10.1038/ncomms1737
94. Tian X, Wang L, Wei J, Yang S, Wang W, Xu Z, Bai X (2014) Filament growth dynamics in solid electrolyte-based resistive memories revealed by in situ TEM. Nano Res 7:1065–1072. doi:10.1007/s12274-014-0469-0
95. Peng S, Zhuge F, Chen X, Zhu X, Hu B, Pan L, Chen B, Li R-W (2012) Mechanism for resistive switching in an oxide-based electrochemical metallization memory. Appl Phys Lett 100:072101. doi:10.1063/1.3683523
96. Kwon D-H, Kim KM, Jang JH, Jeon JM, Lee MH, Kim GH, Li X-S, Park G-S, Lee B, Han S, Kim M, Hwang CS (2010) Atomic structure of conducting nanofilaments in TiO2 resistive switching memory. Nat Nanotechnol 5:148–53. doi:10.1038/nnano.2009.456
97. Inglis AD, Le Page Y, Strobel P, Hurd CM, Search H, Journals C, Contact A, Iopscience M, Phys SS, Address IP (1983) Electrical conductance of crystalline Ti, Oz, for. J Phys C 16:317. doi:10.1088/0022-3719/16/2/015
98. Kwon J, Picard YN, Skowronski M, Sharma AA, Bain JA (2014) In situ biasing TEM investigation of resistive switching events in TiO_2-based RRAM. IEEE Int. Reliab. Phys. Symp. pp 5E.5.1–5E.5.5. doi:10.1109/IRPS.2014.6860680
99. Yoon KJ, Lee MH, Kim GH, Song SJ, Seok JY, Han S, Yoon JH, Kim KM, Hwang CS (2012) Memristive tri-stable resistive switching at ruptured conducting filaments of a Pt/TiO_2/Pt cell. Nanotechnology 23:185202. doi:10.1088/0957-4484/23/18/185202
100. Yoon KJ, Song SJ, Seok JY, Yoon JH, Park TH, Kwon DE, Hwang CS (2014) Evolution of the shape of the conducting channel in complementary resistive switching transition metal oxides. Nanoscale 6:2161–9. doi:10.1039/c3nr05426h
101. Wriedt HA (1987) The O−Zn (oxygen-zinc) system. J Phase Equilibria 8:166–176. doi:10.1007/BF02873202
102. Gu T. Metallic filament formation by aligned oxygen vacancies in ZnO-based resistive switches. J Appl Phys. doi: 10.1063/1.4879677
103. Zhao J, Dong J-Y, Zhao X, Chen W (2014) Role of oxygen vacancy arrangement on the formation of a conductive filament in a ZnO thin film. Chinese Phys Lett 31:057307. doi:10.1088/0256-307X/31/5/057307
104. Strachan JP, Pickett MD, Yang JJ, Aloni S, Kilcoyne ALD, Medeiros-Ribeiro G, Williams RS (2010) Direct identification of the conducting channels in a functioning memristive device. Adv Mater 22:3573–3577. doi:10.1002/adma.201000186
105. Strachan JP, Yang JJ, Montoro L a, Ospina C a, Ramirez a J, Kilcoyne a LD, Medeiros-Ribeiro G, Williams RS (2013) Characterization of electroforming-free titanium dioxide memristors. Beilstein J Nanotechnol 4:467–73. doi:10.3762/bjnano.4.55
106. Strachan JP, Strukov DB, Borghetti J, Yang JJ, Medeiros-Ribeiro G, Williams RS (2011) The switching location of a bipolar memristor: chemical, thermal and structural mapping. Nanotechnology 22:254015. doi:10.1088/0957-4484/22/25/254015

107. Yao J, Zhong L, Natelson D, Tour JM (2012) In situ imaging of the conducting filament in a silicon oxide resistive switch. Sci Rep 2:242. doi:10.1038/srep00242
108. Peng C-N, Wang C-W, Chan T-C, Chang W-Y, Wang Y-C, Tsai H-W, Wu W-W, Chen L-J, Chueh Y-L (2012) Resistive switching of Au/ZnO/Au resistive memory: an in situ observation of conductive bridge formation. Nanoscale Res Lett 7:559. doi:10.1186/1556-276X-7-559
109. Shi L, Shang DS, Chen YS, Wang J, Sun JR, Shen BG (2011) Improved resistance switching in ZnO-based devices decorated with Ag nanoparticles. J Phys D Appl Phys 44:455305. doi:10.1088/0022-3727/44/45/455305
110. Xu DL, Xiong Y, Tang MH, Zeng BW, Li JQ, Liu L, Li LQ, Yan SA, Tang ZH (2014) Bipolar resistive switching behaviors in Cr-doped ZnO films. Microelectron Eng 116:22–25. doi:10.1016/j.mee.2013.11.007
111. Li C, Ding X, Deng C, Bao D (2013) Observing the resistive switching of MgZnO thin film via conducting atomic force microscopy. J Nanosci Nanotechnol 13:766–770. doi:10.1166/jnn.2013.6096
112. Kinoshtia K, Hinoki T, Yazawa K, Ohmi K, Kishida S (2010) Mechanism of resistive memory effect in Ga doped ZnO thin films. Phys Status Solidi 7:1712–1714. doi:10.1002/pssc.200983253
113. Kinoshita K, Okutani T, Tanaka H, Hinoki T, Agura H, Yazawa K, Ohmi K, Kishida S (2011) Flexible and transparent ReRAM with GZO memory layer and GZO-electrodes on large PEN sheet. Solid State Electron 58:48–53. doi:10.1016/j.sse.2010.11.026
114. Moreno C, Munuera C, Obradors X, Ocal C (2012) The memory effect of nanoscale memristors investigated by conducting scanning probe microscopy methods. Beilstein J Nanotechnol 3:722–30. doi:10.3762/bjnano.3.82
115. Janotti A, Van de Walle CG (2007) Native point defects in ZnO. Phys Rev B 76:165202. doi:10.1103/PhysRevB.76.165202
116. Jeong SH, Boo JH (2004) Influence of target-to-substrate distance on the properties of AZO films grown by RF magnetron sputtering. Thin Solid Films 447-448:105–110. doi:10.1016/j.tsf.2003.09.031
117. Lin C-L, Tang C-C, Wu S-C, Juan P-C, Kang T-K (2015) Impact of oxygen composition of ZnO metal-oxide on unipolar resistive switching characteristics of Al/ZnO/Al resistive RAM (RRAM). Microelectron Eng 136:15–21. doi:10.1016/j.mee.2015.03.027
118. Chang W-Y, Lai Y-C, Wu T-B, Wang S-F, Chen F, Tsai M-J (2008) Unipolar resistive switching characteristics of ZnO thin films for nonvolatile memory applications. Appl Phys Lett 92:022110. doi:10.1063/1.2834852
119. Xu N, Liu LF, Sun X, Chen C, Wang Y, Han DD, Liu XY, Han RQ, Kang JF, Yu B (2008) Bipolar switching behavior in TiN/ZnO/Pt resistive nonvolatile memory with fast switching and long retention. Semicond Sci Technol 23:075019. doi:10.1088/0268-1242/23/7/075019
120. Han Y, Cho K, Kim S (2011) Characteristics of multilevel bipolar resistive switching in Au/ZnO/ITO devices on glass. Microelectron Eng 88:2608–2610. doi:10.1016/j.mee.2011.02.058
121. Lin C-L, Tang C-C, Wu S-C, Yang S-R, Lai Y-H, Wu S-C (2011) Resistive switching characteristics of zinc oxide (ZnO) resistive RAM with Al metal electrode. IEEE 4th International Nanoelectronics Conference (INEC). pp 1–2. doi:10.1109/INEC.2011.5991798
122. Chiu F-C, Li P-W, Chang W-Y (2012) Reliability characteristics and conduction mechanisms in resistive switching memory devices using ZnO thin films. Nanoscale Res Lett 7:178. doi:10.1186/1556-276X-7-178
123. Shi W, Tai Q, Xia X-H, Yi M-D, Xie L-H, Fan Q-L, Wang L-H, Wei A, Huang W (2012) Unipolar resistive switching effects based on Al/ZnO/P ++ -Si diodes for nonvolatile memory applications. Chinese Phys Lett 29:087201. doi:10.1088/0256-307X/29/8/087201
124. Jianwei Zhao JZ, Fengjuan Liu FL, Jian Sun JS, Haiqin Huang HH, Zuofu Hu ZH, Xiqing Zhang XZ (2012) Low power consumption bipolar resistive switching characteristics of ZnO-based memory devices. Chinese Opt Lett 10:013102–13105. doi:10.3788/COL201210.013102
125. Muhammad NM, Duraisamy N, Rahman K, Dang HW, Jo J, Choi KH (2013) Fabrication of printed memory device having zinc-oxide active nano-layer and investigation of resistive switching. Curr Appl Phys 13:90–96. doi:10.1016/j.cap.2012.06.017
126. Wang J, Song Z, Xu K, Liu M (2010) Rectifying switching characteristics of Pt/ZnO/Pt structure based resistive memory. J Nanosci Nanotechnol 10:7088–7091. doi:10.1166/jnn.2010.2758
127. Liu Z-J, Chou J-C, Wei S-Y, Gan J-Y, Yew T-R (2011) Improved resistive switching of textured ZnO thin films grown on Ru electrodes. IEEE Electron Device Lett 32:1728–1730. doi:10.1109/LED.2011.2167710
128. Li HX, Shen DD, Ke WQ, Xi JH, Kong Z, Ji ZG (2014) Fabrication and characterization of transparent ZnO film based resistive switching devices. Key Eng Mater 609-610:565–570. doi:10.4028/www.scientific.net/KEM.609-610.565
129. Ji Z, Mao Q, Ke W (2010) Effects of oxygen partial pressure on resistive switching characteristics of ZnO thin films by DC reactive magnetron sputtering. Solid State Commun 150:1919–1922. doi:10.1016/j.ssc.2010.07.032
130. Kang YH, Choi J-H, Lee TI, Lee W, Myoung J-M (2011) Thickness dependence of the resistive switching behavior of nonvolatile memory device structures based on undoped ZnO films. Solid State Commun 151:1739–1742. doi:10.1016/j.ssc.2011.08.036
131. Mao Q, Ji Z, Xi J (2010) Realization of forming-free ZnO-based resistive switching memory by controlling film thickness. J Phys D Appl Phys 43:395104. doi:10.1088/0022-3727/43/39/395104
132. Huang Y, Shen Z, Wu Y, Wang X, Zhang S, Shi X, Zeng H (2016) Amorphous ZnO based resistive random access memory. RSC Adv 6:17867–17872. doi:10.1039/C5RA22728C
133. Huang R, Sun K, Kiang KS, Morgan KA, de Groot CH (2016) Forming-free resistive switching of tunable ZnO films grown by atomic layer deposition. Microelectron Eng 161:7–12. doi:10.1016/j.mee.2016.03.038
134. Li H, Niu B, Mao Q, Xi J, Ke W, Ji Z (2012) Resistive switching characteristics of ZnO based ReRAMs with different annealing temperatures. Solid State Electron 75:28–32. doi:10.1016/j.sse.2012.04.032
135. Zhang F, Li X, Gao X, Wu L, Zhuge F, Wang Q, Liu X, Yang R, He Y (2012) Effect of defect content on the unipolar resistive switching characteristics of ZnO thin film memory devices. Solid State Commun 152:1630–1634. doi:10.1016/j.ssc.2012.04.073
136. Fan Y-S, Liu P-T, Teng L-F, Hsu C-H (2012) Bipolar resistive switching characteristics of Al-doped zinc tin oxide for nonvolatile memory applications. Appl Phys Lett 101:052901. doi:10.1063/1.4742737
137. Shirolkar MM, Hao C, Yin S, Li M, Wang H (2013) Influence of surface null potential on nonvolatile bistable resistive switching memory behavior of dilutely aluminum doped ZnO thin film. Appl Phys Lett 102:243501. doi:10.1063/1.4811256
138. Chu D, Younis A, Li S (2012) Enhancement of resistance switching in electrodeposited Co-ZnO films. ISRN Nanotechnol 2012:1–4. doi:10.5402/2012/705803
139. Chen G, Song C, Chen C, Gao S, Zeng F, Pan F (2012) Resistive switching and magnetic modulation in cobalt-doped ZnO. Adv Mater 24:3515–20. doi:10.1002/adma.201201595
140. Min CK, Keun YL, Chang OK, Suk-Ho C (2011) Effect of doping concentration on resistive switching behaviors of Cu-doped ZnO films. J Korean Phys Soc 59:304. doi:10.3938/jkps.59.304
141. Fan Y-S, Liu P-T, Hsu C-H (2013) Investigation on amorphous InGaZnO based resistive switching memory with low-power, high-speed, high reliability. Thin Solid Films 549:54–58. doi:10.1016/j.tsf.2013.09.033
142. Hu W, Zou L, Chen X, Qin N, Li S, Bao D (2014) Highly uniform resistive switching properties of amorphous InGaZnO thin films prepared by a low temperature photochemical solution deposition method. ACS Appl Mater Interfaces 6:5012–7. doi:10.1021/am500048y
143. Kim M-S, Hwan Hwang Y, Kim S, Guo Z, Moon D-I, Choi J-M, Seol M-L, Bae B-S, Choi Y-K (2012) Effects of the oxygen vacancy concentration in InGaZnO-based resistance random access memory. Appl Phys Lett 101:243503. doi:10.1063/1.4770073
144. Tang MH, Zeng ZQ, Li JC, Wang ZP, Xu XL, Wang GY, Zhang LB, Yang SB, Xiao YG, Jiang B (2011) Resistive switching behavior of La-doped ZnO films for nonvolatile memory applications. Solid State Electron 63:100–104. doi:10.1016/j.sse.2011.05.023
145. Cheng H-C, Chen S-W, Wu J-M (2011) Resistive switching behavior of (Zn1−xMgx)O films prepared by sol–gel processes. Thin Solid Films 519:6155–6159. doi:10.1016/j.tsf.2011.04.013
146. Chao Yang Y, Pan F, Zeng F (2010) Bipolar resistance switching in high-performance Cu/ZnO:Mn/Pt nonvolatile memories: active region and influence of Joule heating. New J Phys 12:023008. doi:10.1088/1367-2630/12/2/023008
147. Peng H, Wu T (2009) Nonvolatile resistive switching in spinel ZnMn[sub 2]O[sub 4] and ilmenite ZnMnO[sub 3]. Appl Phys Lett 95:152106. doi:10.1063/1.3249630
148. Han Y, Cho K, Park S, Kim S (2014) The effects of Mn-doping and electrode material on the resistive switching characteristics of ZnO x S 1-x thin films on plastic. Trans Electr Electron Mater 15:24–27. doi:10.4313/TEEM.2014.15.1.24
149. Huang T-H, Yang P-K, Chang W-Y, Chien J-F, Kang C-F, Chen M-J, He J-H (2013) Eliminating surface effects via employing nitrogen doping

to significantly improve the stability and reliability of ZnO resistive memory. J Mater Chem C 1:7593. doi:10.1039/c3tc31542h

150. Younis A, Chu D, Li S (2013) Bi-stable resistive switching characteristics in Ti-doped ZnO thin films. Nanoscale Res Lett 8:154. doi:10.1186/1556-276X-8-154
151. Li H, Chen Q, Chen X, Mao Q, Xi J, Ji Z (2013) Improvement of resistive switching in ZnO film by Ti doping. Thin Solid Films 537:279–284. doi:10.1016/j.tsf.2013.04.028
152. Yang YC, Pan F, Liu Q, Liu M, Zeng F (2009) Fully room-temperature-fabricated nonvolatile resistive memory for ultrafast and high-density memory application. Nano Lett 9:1636–1643. doi:10.1021/nl900006g
153. Chen X, Hu W, Wu S, Bao D (2014) Complementary switching on TiN/MgZnO/ZnO/Pt bipolar memory devices for nanocrossbar arrays. J Alloys Compd 615:566–568. doi:10.1016/j.jallcom.2014.06.200
154. Lin S-M, Huang J-S, Chang W-C, Hou T-C, Huang H-W, Huang C-H, Lin S-J, Chueh Y-L (2013) Single-step formation of ZnO/ZnWO(x) bilayer structure via interfacial engineering for high performance and low energy consumption resistive memory with controllable high resistance states. ACS Appl Mater Interfaces 5:7831–7. doi:10.1021/am4016928
155. Chen G, Song C, Pan F (2013) Improved resistive switching stability of Pt/ZnO/CoO x/ZnO/Pt structure for nonvolatile memory devices. Rare Met 32: 544–549. doi:10.1007/s12598-013-0080-7
156. Xu D, Xiong Y, Tang M, Zeng B, Xiao Y, Li J, Liu L, Yan S, Tang Z, Wang L, Zhu X, Li R (2013) Improvement of resistive switching performances in ZnLaO film by embedding a thin ZnO buffer layer. ECS Solid State Lett 2:Q69–Q71. doi:10.1149/2.002309ssl
157. Zhu Y, Li M, Zhou H, Hu Z, Liu X, Liao H (2013) Improved bipolar resistive switching properties in CeO 2/ZnO stacked heterostructures. Semicond Sci Technol 28:015023. doi:10.1088/0268-1242/28/1/015023
158. Chang L-C, Kao H-L, Liu K-H (2014) Effect of annealing treatment on the electrical characteristics of Pt/Cr-embedded ZnO/Pt resistance random access memory devices. J Vac Sci Technol A Vacuum, Surfaces, Film 32:02B119. doi:10.1116/1.4865551
159. Qin S-C, Dong R-X, Yan X-L (2014) Memristive behavior of ZnO film with embedded Ti nano-layers. Appl Phys A 116:1–7. doi:10.1007/s00339-014-8450-z
160. Baghini MS, Kumar A (2014) Experimental study for selection of electrode material for ZnO-based memristors. Electron Lett 50:1547–1549. doi:10.1049/el.2014.1491
161. Xue WH, Xiao W, Shang J, Chen XX, Zhu XJ, Pan L, Tan HW, Zhang WB, Ji ZH, Liu G, Xu X-H, Ding J, Li R-W (2014) Intrinsic and interfacial effect of electrode metals on the resistive switching behaviors of zinc oxide films. Nanotechnology 25:425204. doi:10.1088/0957-4484/25/42/425204
162. Chang W-Y, Peng C-S, Lin C-H, Tsai J-M, Chiu F-C, Chueh Y-L (2011) Polarity of bipolar resistive switching characteristics in ZnO memory films. J Electrochem Soc 158:H872. doi:10.1149/1.3603989
163. Chang W-Y, Huang H-W, Wang W-T, Hou C-H, Chueh Y-L, He J-H (2012) High uniformity of resistive switching characteristics in a Cr/ZnO/Pt device. J Electrochem Soc 159:G29–G32. doi:10.1149/2.092203jes
164. Xu N, Liu L, Sun X, Liu X, Han D, Wang Y, Han R, Kang J, Yu B (2008) Characteristics and mechanism of conduction/set process in TiN / ZnO / Pt resistance switching random-access memories. Appl Phys Lett 92:232112. doi:10.1063/1.2945278
165. Liu K-C, Tzeng W-H, Chang K-M, Wu C-H (2010) The effect of plasma deposition on the electrical characteristics of Pt/HfOx/TiN RRAM device. Surf Coatings Technol 205:S379–S384. doi:10.1016/j.surfcoat.2010.08.043
166. Hsieh WK, Lam KT, Chang SJ (2015) Bipolar Ni/ZnO/HfO2/Ni RRAM with multilevel characteristic by different reset bias. Mater Sci Semicond Process 35:30–33. doi:10.1016/j.mssp.2015.02.073
167. Zoolfakar AS, Ab Kadir R, Rani RA, Balendhran S, Liu X, Kats E, Bhargava SK, Bhaskaran M, Sriram S, Zhuiykov S, O'Mullane AP, Kalantar-zadeh K (2013) Engineering electrodeposited ZnO films and their memristive switching performance. Phys Chem Chem Phys 15:10376. doi:10.1039/c3cp44451a
168. Wang Y-P, Lee W-I, Tseng T-Y (1996) Degradation phenomena of multilayer ZnO–glass varistors studied by deep level transient spectroscopy. Appl Phys Lett 69:1807. doi:10.1063/1.117493
169. Simanjuntak FM, Prasad OK, Panda D, Lin C-A, Tsai T-L, Wei K-H, Tseng T-Y (2016) Impacts of Co doping on ZnO transparent switching memory device characteristics. Appl Phys Lett 108:183506. doi:10.1063/1.4948598
170. Zhang J, Yang H, Zhang Q, Dong S, Luo JK (2013) Structural, optical, electrical and resistive switching properties of ZnO thin films deposited by thermal and plasma-enhanced atomic layer deposition. Appl Surf Sci 282:390–395. doi:10.1016/j.apsusc.2013.05.141
171. Zhang J, Yang H, Zhang Q, Jiang H, Luo J, Zhou J, Dong S (2014) Resistive switching of in situ and ex situ oxygen plasma treated ZnO thin film deposited by atomic layer deposition. Appl Phys A 663–669. doi: 10.1007/s00339-014-8324-4
172. Zhang J, Yang H, Zhang Q, Dong S, Luo JK (2013) Bipolar resistive switching characteristics of low temperature grown ZnO thin films by plasma-enhanced atomic layer deposition. Appl Phys Lett 102:012113. doi:10.1063/1.4774400
173. Bae S, Kim D-S, Jung S, Jeong W, Lee J, Cho S, Park J, Byun D (2015) Bipolar switching behavior of ZnO x thin films deposited by metalorganic chemical vapor deposition at various growth temperatures. J Electron Mater 44:4175–4181. doi:10.1007/s11664-015-3935-x
174. Deshpande S, Nair VV (2009) Resistive switching of Al/Sol-Gel ZnO/Al devices for resistive random access memory applications. Int Conf Adv Comput Control Telecommun Technol 2009:471–473. doi:10.1109/ACT.2009.122
175. Lee W-H, Kim E-J, Yoon S-M (2015) Effect of Al incorporation amount upon the resistive-switching characteristics for nonvolatile memory devices using Al-doped ZnO semiconductors. J Vac Sci Technol B, Nanotechnol Microelectron Mater Process Meas Phenom 33:051216. doi:10.1116/1.4930896
176. Yu H, Kim M, Kim Y, Lee J, Kim K, Choi S, Cho S (2014) Al-doped ZnO as a switching layer for transparent bipolar resistive switching memory. Electron Mater Lett 10:321–324. doi:10.1007/s13391-013-3225-9
177. Chiu F-C (2014) Conduction mechanisms in resistance switching memory devices using transparent boron doped zinc oxide films. Materials (Basel) 7:7339–7348. doi:10.3390/ma7117339
178. Xu H, Kim DH, Xiahou Z, Li Y, Zhu M, Lee B, Liu C (2016) Effect of Co doping on unipolar resistance switching in Pt/Co:ZnO/Pt structures. J Alloys Compd 658:806–812. doi:10.1016/j.jallcom.2015.11.018
179. Jia CH, Dong QC, Zhang WF (2012) Effect of incorporating copper on resistive switching properties of ZnO films. J Alloys Compd 520:250–254. doi:10.1016/j.jallcom.2012.01.035
180. Zhang Y, Duan Z, Li R, Ku C-J, Reyes P, Ashrafi A, Lu Y (2012) FeZnO-based resistive switching devices. J Electron Mater 41:2880–2885. doi:10.1007/s11664-012-2045-2
181. Hu W, Chen X, Wu G, Lin Y, Qin N, Bao D (2012) Bipolar and tri-state unipolar resistive switching behaviors in Ag/ZnFe2O4/Pt memory devices. Appl Phys Lett 101:63501. doi:10.1063/1.4744950
182. Zhao J-W, Sun J, Huang H-Q, Liu F-J, Hu Z-F, Zhang X-Q (2012) Effects of ZnO buffer layer on GZO RRAM devices. Appl Surf Sci 258:4588–4591. doi:10.1016/j.apsusc.2012.01.034
183. Park SP, Yoon DH, Tak YJ, Lee H, Kim HJ (2015) Highly reliable switching via phase transition using hydrogen peroxide in homogeneous and multi-layered GaZnO x-based resistive random access memory devices. Chem Commun 51:9173–9176. doi:10.1039/C4CC10209F
184. Igityan A, Kafadaryan Y, Aghamalyan N, Petrosyan S, Badalyan G, Vardanyan V, Nersisyan M, Hovsepyan R, Palagushkin A, Kryzhanovsky B (2015) Resistivity switching properties of Li-doped ZnO fi lms deposited on LaB 6 electrode. Thin Solid Films 595:92–95. doi:10.1016/j.tsf.2015.10.064
185. Lin C-C, Tseng Z-L, Lo K-Y, Huang C-Y, Hong C-S, Chu S-Y, Chang C-C, Wu C-J (2012) Unipolar resistive switching behavior of Pt/LixZn1–xO/Pt resistive random access memory devices controlled by various defect types. Appl Phys Lett 101:203501. doi:10.1063/1.4766725
186. Cao X, Li X, Gao X, Liu X, Yang C, Chen L (2011) Structural properties and resistive switching behaviour in Mg x Zn 1–x O alloy films grown by pulsed laser deposition. J Phys D Appl Phys 44:015302. doi:10.1088/0022-3727/44/1/015302
187. Chen X, Wu G, Bao D (2008) Resistive switching behavior of Pt/Mg[sub 0.2]Zn[sub 0.8]O/Pt devices for nonvolatile memory applications. Appl Phys Lett 93:093501. doi:10.1063/1.2978158
188. Chen X, Wu G, Hu W, Zhou H, Bao D (2012) Comparative investigation of unipolar resistance switching effect of Pt/Mg0.6Zn0.4O/Pt devices with different electrode patterns for nonvolatile memory application. Appl Phys A 108:503–508. doi:10.1007/s00339-012-6924-4
189. Hsieh W-K, Chuang RW, Chang S-J (2015) Two-bit-per-cell resistive switching memory device with a Ti/MgZnO/Pt structure. RSC Adv 5:88166–88170. doi:10.1039/C5RA15993H
190. Wang H, Gao SM, Xu JW, Yang L, Qiu W (2013) Effects of Mg-doping on resistance switching property of $Mg_xZn_{1-x}O$ thin films prepared by sol-gel method. Adv Mater Res 750-752:1034–1037. doi:10.4028/www.scientific.net/AMR.750-752.1034

191. Ren S, Dong J, Zhang L, Huang Y, Guo J, Zhang L, Zhao J, Chen W (2015) Microstructure related quantum conductance in Mn-doped ZnO resistive switching memory. IEEE Magn. Conf. pp 1–1. doi:10.1109/INTMAG.2015.7157752
192. Wang H, Li Z, Xu J, Zhang Y, Yang L, Qiu W (2015) Resistance switching properties of Ag/ZnMn2O4/p-Si fabricated by magnetron sputtering for resistance random access memory. J Wuhan Univ Technol Sci Ed 30:1159–1162. doi:10.1007/s11595-015-1288-1
193. Xu J, Yang Z, Zhang Y, Zhang X, Wang HUA (2014) Bipolar resistive switching behaviours in ZnMn 2 O 4 film deposited on p + -Si substrate by chemical solution deposition. Bull Mater Sci 37:1657–1661. doi:10.1007/s12034-014-0731-9
194. Yang YC, Fan B, Zeng F, Pan F (2010) Bipolar resistance switching characteristics in TiN/ZnO:Mn/Pt junctions developed for nonvolatile resistive memory application. J Nanosci Nanotechnol 10:7370–7373. doi:10.1166/jnn.2010.2762
195. Zhang Y, Wang H, Xu J, Yang L, Qiu W, Li Z (2014) Effect of ZnMn 2 O 4 thickness on its resistive switching characteristics. Indian J Eng Mater Sci 21:563–566
196. Wenxiang S, Kailiang Z, Fang W, Kuo S, Yinping M, Jinshi Z (2013) Resistive switching characteristics of zinc oxide resistive RAM doped with nickel. ECS Trans 52:1009–1014. doi:10.1149/05201.1009ecst
197. Cho K, Park S, Chung I, Kim S (2014) Effect of oxidizable electrode material on resistive switching characteristics of ZnO(x)S(1-x) films. J Nanosci Nanotechnol 14:8187–8190. doi:10.1166/jnn.2014.9881
198. Murali S, Rajachidambaram JS, Han SY, Chang CH, Herman GS, Conley JF (2011) Bipolar resistive switching of zinc-tin-oxide resistive random access memory. Proc IEEE Conf Nanotechnol 740–743. doi: 10.1109/NANO.2011.6144646
199. Zheng K, Zhao JL, Leck KS, Teo KL, Yeo EG, Sun XW (2014) A ZnTaOx based resistive switching random access memory. ECS Solid State Lett 3:Q36–Q39. doi:10.1149/2.0101407ssl
200. Fan Y-S, Chan W-L, Chang C-H, Zheng G-T, Chang C-C, Liu P-T (2015) Performance and reliability of non-linear Al-Zn-Sn-O based resistive random access memory. IEEE 22nd Int. Symp Phys Fail Anal Integr Circuits. pp 381–384. doi:10.1109/IPFA.2015.7224421
201. Oh D, Yun DY, Lee NH, Kim TW (2015) Resistive switching characteristics and conduction mechanisms of nonvolatile memory devices based on Ga and Sn co-doped ZnO films. Thin Solid Films 587:71–74. doi:10.1016/j.tsf.2014.12.021
202. Chen MC, Chang TC, Huang SY, Sze SM, Tsai MJ (2011) Studies on nonvolatile resistance memory switching behaviors in InGaZnO thin films. 2011 11th Annu Non-Volatile Mem Technol Symp NVMTS 2011 :96–99. doi: 10.1109/NVMTS.2011.6137093
203. Chen M-C, Chang T-C, Huang S-Y, Chang G-C, Chen S-C, Huang H-C, Hu C-W, Sze SM, Tsai T-M, Gan D-S, Yeh (Huang) F-S, Tsai M-J (2011) Influence of oxygen partial pressure on resistance random access memory characteristics of indium gallium zinc oxide. Electrochem Solid-State Lett 14:H475. doi:10.1149/2.007112esl
204. Chen M-C, Chang T-C, Tsai C-T, Huang S-Y, Chen S-C, Hu C-W, Sze SM, Tsai M-J (2010) Influence of electrode material on the resistive memory switching property of indium gallium zinc oxide thin films. Appl Phys Lett 96:262110. doi:10.1063/1.3456379
205. Hwang Y, An H, Cho W (2014) Performance improvement of the resistive memory properties of InGaZnO thin films by using microwave irradiation. Jpn J Appl Phys 53:04EJ04–1. doi:10.7567/JJAP.53.04EJ04
206. Kim CH, Jang YH, Hwang HJ, Song CH, Yang YS, Cho JH (2010) Bistable resistance memory switching effect in amorphous InGaZnO thin films. Appl Phys Lett 97:062109. doi:10.1063/1.3479527
207. Pei Y, Mai B, Zhang X, Hu R, Li Y, Chen Z, Fan B, Liang J, Wang G (2014) Forming free bipolar ReRAM of Ag/a-IGZO/Pt with improved resistive switching uniformity through controlling oxygen partial pressure. J Electron Mater 44:645–650. doi:10.1007/s11664-014-3547-x
208. Yan X, Hao H, Chen Y, Shi S, Zhang E, Lou J, Liu B (2014) Self-rectifying performance in the sandwiched structure of Ag/In-Ga-Zn-O/Pt bipolar resistive switching memory. Nanoscale Res Lett 9:548. doi:10.1186/1556-276X-9-548
209. Kröger FA, Vink HJ (1956) Relations between the concentrations of imperfections in crystalline solids. Solid State Phys 3:307–435. doi:10.1016/S0081-1947(08)60135-6
210. Thomas G (1997) Materials science: invisible circuits. Nature 389:907–908. doi:10.1038/39999
211. Wager JF (2003) Applied physics: transparent electronics. Science (80-) 300: 1245–1246. doi:10.1126/science.1085276
212. Seo JW, Park J-W, Lim KS, Yang J-H, Kang SJ (2008) Transparent resistive random access memory and its characteristics for nonvolatile resistive switching. Appl Phys Lett 93:223505. doi:10.1063/1.3041643
213. Shi L, Shang D, Sun J, Shen B (2009) Bipolar resistance switching in fully transparent ZnO:Mg-based devices. Appl Phys Express 2:101602. doi:10.1143/APEX.2.101602
214. Kim A, Song K, Kim Y, Moon J (2011) All solution-processed, fully transparent resistive memory devices. ACS Appl Mater Interfaces 3:4525–30. doi:10.1021/am201215e
215. Gao S, Wang H, Xu J, Yuan C, Zhang X (2012) Effect of annealing temperature on resistance switching behavior of Mg0.2Zn0.8O thin films deposited on ITO glass. Solid State Electron 76:40–43. doi:10.1016/j.sse.2012.05.009
216. Huang CY, Ho YT, Hung CJ, Tseng TY (2014) Compact Ga-Doped ZnO Nanorod Thin Film for Making High-Performance Transparent Resistive Switching Memory. IEEE Trans Electron Devices. 1–6. doi: 10.1109/TED.2014.2343631
217. Yang P-K, Chang W-Y, Teng P-Y, Jeng S-F, Lin S-J, Chiu P-W, He J-H (2013) Fully transparent resistive memory employing graphene electrodes for eliminating undesired surface effects. Proc IEEE 101:1732–1739. doi:10.1109/JPROC.2013.2260112
218. Zhang R, Miao J, Shao F, Huang WT, Dong C, Xu XG, Jiang Y (2014) Transparent amorphous memory cell: a bipolar resistive switching in ZnO/Pr0.7Ca0.3MnO3/ITO for invisible electronics application. J Non Cryst Solids 406:102–106. doi:10.1016/j.jnoncrysol.2014.09.055
219. Simanjuntak FM, Panda D, Tsai T-L, Lin C-A, Wei K-H, Tseng T-Y (2015) Enhancing the memory window of AZO/ZnO/ITO transparent resistive switching devices by modulating the oxygen vacancy concentration of the top electrode. J Mater Sci 50:6961–6969. doi:10.1007/s10853-015-9247-y
220. Wu X, Xu Z, Yu Z, Zhang T, Zhao F, Sun T, Ma Z, Li Z, Wang S (2015) Resistive switching behavior of photochemical activation solution-processed thin films at low temperatures for flexible memristor applications. J Phys D Appl Phys 48:115101. doi:10.1088/0022-3727/48/11/115101
221. Cao X, Li X, Gao X, Liu X, Yang C, Yang R, Jin P (2011) All-ZnO-based transparent resistance random access memory device fully fabricated at room temperature. J Phys D Appl Phys 44:255104. doi:10.1088/0022-3727/44/25/255104
222. Misra P, Das AK, Kukreja LM (2010) Switching characteristics of ZnO based transparent resistive random access memory devices grown by pulsed laser deposition. Phys Status Solidi 7:1718–1720. doi:10.1002/pssc.200983244
223. Zheng K, Sun XW, Zhao JL, Wang Y, Yu HY, Demir HV, Teo KL (2011) An indium-free transparent resistive switching random access memory. IEEE Electron Device Lett 32:797–799. doi:10.1109/LED.2011.2126017
224. Wang Y (2012) Resistive-switching mechanism of transparent nonvolatile memory device based on gallium zinc oxide. Phys Status Solidi 209:364–368. doi:10.1002/pssa.201127391
225. Zhong C-W, Tzeng W-H, Liu K-C, Lin H-C, Chang K-M, Chan Y-C, Kuo C-C, Chen P-S, Lee H-Y, Chen F, Tsai M-J (2013) Effect of ITO electrode with different oxygen contents on the electrical characteristics of HfOx RRAM devices. Surf Coatings Technol 231:563–566. doi:10.1016/j.surfcoat.2012.07.039
226. Ye C, Deng T, Wu J, Zhan C, Wang H, Zhang J (2015) Role of ITO electrode in the resistive switching behavior of TiN/HfO2/ITO memory devices at different annealing temperatures. Jpn J Appl Phys 54:054201. doi:10.7567/JJAP.54.054201
227. Wu X, Xu H, Wang Y, Rogach AL, Shen Y, Zhao N (2015) General observation of the memory effect in metal-insulator-ITO structures due to indium diffusion. Semicond Sci Technol 30:074002. doi:10.1088/0268-1242/30/7/074002
228. Seo JW, Baik SJ, Kang SJ, Lim KS (2011) Fabrication of Semi-transparent Resistive Random Access memory and Its Characteristics of Nonvolatile Resistive Switching. MRS Proc 1292:mrsf10–1292–k08–21. doi: 10.1557/opl.2011.152
229. Gergel-Hackett N, Tedesco JL, Richter C a (2012) Memristors with flexible electronic applications. Proc IEEE 100:1971–1978. doi:10.1109/JPROC.2011.2158284
230. Khurana G, Misra P, Kumar N, Katiyar RS (2014) Tunable power switching in nonvolatile flexible memory devices based on graphene oxide embedded with ZnO nanorods. J Phys Chem C 118:21357–21364. doi:10.1021/jp506856f
231. Shi L, Shang D-S, Sun J-R, Shen B-G (2010) Flexible resistance memory devices based on Cu/ZnO:Mg/ITO structure. Phys status solidi - Rapid Res Lett 4:344–346. doi:10.1002/pssr.201004364
232. Kim S, Moon H, Gupta D, Yoo S, Choi Y-K (2009) Resistive switching characteristics of sol–gel zinc oxide films for flexible memory Applications1. IEEE Trans IEEE Trans Electron Devices 56:696–699. doi:10.1109/TED.2009.2012522

233. Won Seo J, Park J-W, Lim KS, Kang SJ, Hong YH, Yang JH, Fang L, Sung GY, Kim H-K (2009) Transparent flexible resistive random access memory fabricated at room temperature. Appl Phys Lett 95:133508. doi:10.1063/1.3242381
234. Park S, Lee JH, Kim H-D, Hong SM, An H-M, Kim TG (2013) Resistive switching characteristics of sol-gel based ZnO nanorods fabricated on flexible substrates. Phys status solidi - Rapid Res Lett 7:493–496. doi:10.1002/pssr.201307187
235. Zhou H, Fang G-J, Zhu Y, Liu N, Li M, Zhao X-Z (2011) Flexible resistive switching memory based on Mn 0.20 Zn 0.80 O/HfO 2 bilayer structure. J Phys D Appl Phys 44:445101. doi:10.1088/0022-3727/44/44/445101
236. Fan Y-S, Liu P-T, Hsu C-H, Lai H-Y (2012) P-76: resistive switching memory device based on amorphous Al-Zn-Sn-O film for flexible electronics application. SID Symp Dig Tech Pap 43:1340–1342. doi:10.1002/j.2168-0159.2012.tb06051.x
237. Lee S, Kim H, Yun D-J, Rhee S-W, Yong K (2009) Resistive switching characteristics of ZnO thin film grown on stainless steel for flexible nonvolatile memory devices. Appl Phys Lett 95:262113. doi:10.1063/1.3280864
238. Han S-T, Zhou Y, Roy V a L (2013) Towards the development of flexible non-volatile memories. Adv Mater 25:5425–49. doi:10.1002/adma.201301361
239. Wu J-L, Chen Y-C, Lin H-Y, Chu S-Y, Chang C-C, Wu C-J, Juang Y-D (2013) Effect of ZnO buffer layer on the bending durability of ZnO:Ga films grown on flexible substrates: investigation of surface energy, electrical, optical, and structural properties. IEEE Trans Electron Devices 60:2324–2330. doi:10.1109/TED.2013.2259491
240. Wang ZQ, Xu HY, Li XH, Zhang XT, Liu YX, Liu YC (2011) Flexible resistive switching memory device based on amorphous InGaZnO film with excellent mechanical endurance. IEEE Electron Device Lett 32:1442–1444. doi:10.1109/LED.2011.2162311
241. Linn E, Rosezin R, Kügeler C, Waser R (2010) Complementary resistive switches for passive nanocrossbar memories. Nat Mater 9:403–6. doi:10.1038/nmat2748
242. Lee MJ, Seo S, Kim DC, Ahn SE, Seo DH, Yoo IK, Baek IG, Kim DS, Byun IS, Kim SH, Hwang IR, Kim JS, Jeon SH, Park BH (2007) A low-temperature-grown oxide diode as a new switch element for high-density, nonvolatile memories. Adv Mater 19:73–76. doi:10.1002/adma.200601025
243. Shin YC, Song J, Kim KM, Choi BJ, Choi S, Lee HJ, Kim GH, Eom T, Hwang CS (2008) (In,Sn)[sub 2]O[sub 3] / TiO[sub 2] / Pt Schottky-type diode switch for the TiO[sub 2] resistive switching memory array. Appl Phys Lett 92:162904. doi:10.1063/1.2912531
244. Park WY, Kim GH, Seok JY, Kim KM, Song SJ, Lee MH, Hwang CS (2010) A Pt/TiO 2/Ti Schottky-type selection diode for alleviating the sneak current in resistance switching memory arrays. Nanotechnology 21:195201. doi:10.1088/0957-4484/21/19/195201
245. Lee M-J, Park Y, Suh D-S, Lee E-H, Seo S, Kim D-C, Jung R, Kang B-S, Ahn S-E, Lee CB, Seo DH, Cha Y-K, Yoo I-K, Kim J-S, Park BH (2007) Two series oxide resistors applicable to high speed and high density nonvolatile memory. Adv Mater 19:3919–3923. doi:10.1002/adma.200700251
246. Lee M-J, Kim SI, Lee CB, Yin H, Ahn S-E, Kang BS, Kim KH, Park JC, Kim CJ, Song I, Kim SW, Stefanovich G, Lee JH, Chung SJ, Kim YH, Park Y (2009) Low-temperature-grown transition metal oxide based storage materials and oxide transistors for high-density non-volatile memory. Adv Funct Mater 19:1587–1593. doi:10.1002/adfm.200801032
247. Won Seo J, Baik SJ, Kang SJ, Hong YH, Yang JH, Lim KS (2011) A ZnO cross-bar array resistive random access memory stacked with heterostructure diodes for eliminating the sneak current effect. Appl Phys Lett 98:233505. doi:10.1063/1.3599707
248. Zhang Y, Duan Z, Li R, Ku C-J, Reyes PI, Ashrafi A, Zhong J, Lu Y (2013) Vertically integrated ZnO-Based 1D1R structure for resistive switching. J Phys D Appl Phys 46:145101. doi:10.1088/0022-3727/46/14/145101
249. Flocke A, Noll TG (2007) Fundamental analysis of resistive nano-crossbars for the use in hybrid Nano/CMOS-memory. ESSCIRC 2007 - 33rd Eur Solid-State Circuits Conf :328–331. doi: 10.1109/ESSCIRC.2007.4430310
250. Shen G-H, Tandio AR, Lin M-Y, Lin G-F, Chen K-H, Hong FC-N. Low Switching-Threshold-Voltage Zinc Oxide Nanowire Array Resistive Random Access Memory. Thin Solid Films doi: 10.1016/j.tsf.2016.04.027
251. Dongale TD, Khot KV, Mali SS, Patil PS, Gaikwad PK, Kamat RK, Bhosale PN (2015) Development of Ag/ZnO/FTO thin film memristor using aqueous chemical route. Mater Sci Semicond Process 40:523–526. doi:10.1016/j.mssp.2015.07.004
252. Chang W-Y, Lin C-A, He J-H, Wu T-B (2010) Resistive switching behaviors of ZnO nanorod layers. Appl Phys Lett 96:242109. doi:10.1063/1.3453450
253. Tseng Z-L, Kao P-C, Shih M-F, Huang H-H, Wang J-Y, Chu S-Y (2010) Electrical bistability in hybrid ZnO nanorod/polymethylmethacrylate heterostructures. Appl Phys Lett 97:212103. doi:10.1063/1.3511756
254. Yao I-C, Lee D-Y, Tseng T-Y, Lin P (2012) Fabrication and resistive switching characteristics of high compact Ga-doped ZnO nanorod thin film devices. Nanotechnology 23:145201. doi:10.1088/0957-4484/23/14/145201
255. Park J, Lee S, Yong K (2012) Photo-stimulated resistive switching of ZnO nanorods. Nanotechnology 23:385707. doi:10.1088/0957-4484/23/38/385707
256. Huang C-H, Huang J-S, Lin S-M, Chang W-Y, He J-H, Chueh Y-L (2012) ZnO1-x nanorod arrays/ZnO thin film bilayer structure: from homojunction diode and high-performance memristor to complementary 1D1R application. ACS Nano 6:8407–14. doi:10.1021/nn303233r
257. Chew ZJ, Li L (2013) A discrete memristor made of ZnO nanowires synthesized on printed circuit board. Mater Lett 91:298–300. doi:10.1016/j.matlet.2012.10.011
258. Bera A, Peng H, Lourembam J, Shen Y, Sun XW, Wu T (2013) A versatile light-switchable nanorod memory: wurtzite ZnO on perovskite SrTiO 3. Adv Funct Mater 23:4977–4984. doi:10.1002/adfm.201300509
259. Yoo EJ, Shin IK, Yoon TS, Choi YJ, Kang CJ (2014) Resistive switching characteristics of ZnO nanowires. J Nanosci Nanotechnol 14:9459–9464. doi:10.1166/jnn.2014.10157
260. Zou C, Wang H, Liang F, Shao L. Reversible switching of ferromagnetism in ZnCuO nanorods by electric field. Appl Phys Lett. doi: 10.1063/1.4915605
261. Sun Y, Yan X, Zheng X, Liu Y, Zhao Y, Shen Y, Liao Q, Zhang Y (2015) High On–Off Ratio Improvement of ZnO-Based Forming-Free Memristor by Surface Hydrogen Annealing. ACS Appl Mater Interfaces. 150327123046007. doi: 10.1021/acsami.5b01080
262. Cheng B, Zhao J, Xiao L, Cai Q, Guo R, Xiao Y, Lei S (2015) PMMA interlayer-modulated memory effects by space charge polarization in resistive switching based on CuSCN-nanopyramids/ZnO-nanorods p-n heterojunction. Nat Publ Gr :1–9. doi: 10.1038/srep17859
263. Wang HJ, Zou CW, Zhou L, Tian CX, Lee MK, Lee JC, Kang TW, Fu DJ (2011) Electrical properties and carrier transport mechanisms of nonvolatile memory devices based on randomly oriented ZnO nanowire networks. Phys status solidi - Rapid Res Lett 5:223–225. doi:10.1002/pssr.201105146
264. Li L, Zhang Y, Chew Z (2013) A Cu/ZnO nanowire/Cu resistive switching device. Nano-Micro Lett 3:159–162. doi:10.1007/BF03353745
265. Zhao WX, Sun B, Liu YH, Wei LJ, Li HW, Chen P. Light-controlled resistive switching of ZnWO4 nanowires array. AIP Adv. doi: 10.1063/1.4891461
266. Kapitanova OO, Panin GN, Kononenko OV, Baranov a N, Kang TW (2014) Resistive switching in graphene/graphene oxide/ZnO heterostructures. J Korean Phys Soc 64:1399–1402. doi:10.3938/jkps.64.1399
267. Valanarasu S, Kathalingam A, Rhee J-K, Chandramohan R, Vijayan TA, Karunakaran M (2015) Improved memory effect of ZnO nanorods embedded in an insulating polymethylmethacrylate layer. J Nanosci Nanotechnol 15:1416–1420. doi:10.1166/jnn.2015.9034
268. Yamamoto HM (2014) Sheathed nanowires aligned by crystallographic periodicity: a possibility of cross-bar wiring in three-dimensional space. CrystEngComm 16:2857. doi:10.1039/c3ce41015c
269. Retamal JRD, Kang C-F, Ho C-H, Ke J-J, Chang W-Y, He J-H (2014) Effect of ultraviolet illumination on metal oxide resistive memory. Appl Phys Lett 105:253111. doi:10.1063/1.4904396
270. Shih C, Chang K, Chang T, Tsai T, Zhang R, Chen J, Chen K, Young T, Chen H, Lou J, Chu T, Huang S, Bao D, Sze SM (2014) Resistive switching modification by ultraviolet illumination in transparent electrode resistive random access memory. IEEE Electron Device Lett 35:633–635. doi:10.1109/LED.2014.2316673
271. Huang T-H, Yang P-K, Lien D-H, Kang C-F, Tsai M-L, Chueh Y-L, He J-H (2014) Resistive memory for harsh electronics: immunity to surface effect and high corrosion resistance via surface modification. Sci Rep 4:4402. doi:10.1038/srep04402
272. Ke J-J, Liu Z-J, Kang C-F, Lin S-J, He J-H (2011) Surface effect on resistive switching behaviors of ZnO. Appl Phys Lett 99:192106. doi:10.1063/1.3659296
273. Lee H-J, Jeong S-Y, Cho CR, Park CH (2002) Study of diluted magnetic semiconductor: Co-doped ZnO. Appl Phys Lett 81:4020. doi:10.1063/1.1517405
274. Naeem M, Hasanain SK, Kobayashi M, Ishida Y, Fujimori a, Buzby S, Shah SI (2006) Effect of reducing atmosphere on the magnetism of Zn(1-x)Co(x)O (0≤x≤0.10) nanoparticles. Nanotechnology 17:2675–2680. doi:10.1088/0957-4484/17/10/039

275. Wang L, Zhang F, Xu Z, Zhao S, Lu L (2010) Influence of the cobalt concentration on optical and magnetic properties of zinc oxide. Chinese Sci Bull 55:897–901. doi:10.1007/s11434-009-0732-z
276. Wu W, Wang ZL (2011) Piezotronic nanowire-based resistive switches as programmable electromechanical memories. Nano Lett 11:2779–2785. doi: 10.1021/nl201074a
277. Lu J, Li Z, Yin G, Ge M, He D, Wang H. Lateral photovoltaic effect co-observed with unipolar resistive switching behavior in Cu-doped ZnO film. J Appl Phys. doi: 10.1063/1.4896366
278. Zhao JL, Teo KL, Zheng K, Sun XW (2016) Color tunable electroluminescence and resistance switching from a ZnO-nanorod-TaOx-p-GaN heterojunction. Nanotechnology 27:115204. doi:10.1088/0957-4484/27/11/115204
279. Lim JH, Kong CK, Kim KK, Park IK, Hwang DK, Park SJ (2006) UV electroluminescence emission from ZnO light-emitting diodes grown by high-temperature radiofrequency sputtering. Adv Mater 18:2720–2724. doi:10.1002/adma.200502633
280. Kou LZ, Guo WL, Li C (2008) Piezoelectricity of ZNO and its nanostructures. 2008 Symp Piezoelectricity, Acoust Waves. Device Appl SPAWDA 2008:354–359. doi:10.1109/SPAWDA.2008.4775808
281. Kumar B, Kim SW (2012) Energy harvesting based on semiconducting piezoelectric ZnO nanostructures. Nano Energy 1:342–355. doi:10.1016/j.nanoen.2012.02.001
282. Look DC, Claflin B, Alivov YI, Park SJ (2004) The future of ZnO light emitters. Phys Status Solidi C Conf 1:2203–2212. doi:10.1002/pssa.200404803
283. Prall K, Ramaswamy N, Kinney W, Holtzclaw K, Chen X, Strand J, Bez R (2012) An update on emerging memory: Progress to 2Xnm. 4th IEEE Int. Mem. Work. pp 1–5. doi:10.1109/IMW.2012.6213635
284. Deng R, Yao B, Li YF, Zhao YM, Li BH, Shan CX, Zhang ZZ, Zhao DX, Zhang JY, Shen DZ, Fan XW (2009) X-ray photoelectron spectroscopy measurement of n-ZnO/p-NiO heterostructure valence-band offset. Appl Phys Lett 94:111–114. doi:10.1063/1.3072367
285. Fang L, Baik SJ, Kim JW, Kang SJ, Seo JW, Jeon JW, Kim YH, Lim KS. Tunable work function of a WOx buffer layer for enhanced photocarrier collection of pin-type amorphous silicon solar cells. J Appl Phys. doi: 10.1063/1.3583576
286. Li H, Lv X, Xi J, Wu X, Mao Q, Liu Q, Ji Z (2014) Effects of TiOx interlayer on resistance switching of Pt/TiO x/ZnO/n^+-Si structures. Surf Rev Lett 21: 1450061. doi:10.1142/S0218625X14500619
287. Sekhar KC, Kamakshi K, Bernstorff S, Gomes MJM (2015) Effect of annealing temperature on photoluminescence and resistive switching characteristics of ZnO/Al2O3 multilayer nanostructures. J Alloys Compd 619:248–252. doi:10.1016/j.jallcom.2014.09.067
288. Chen M-C, Chang T-C, Huang S-Y, Chen S-C, Hu C-W, Tsai C-T, Sze SM (2010) Bipolar resistive switching characteristics of transparent indium gallium zinc oxide resistive random access memory. Electrochem Solid-State Lett 13:H191. doi:10.1149/1.3360181
289. Seung-Eon A, Bo Soo K, Ki Hwan K, Myoung-Jae L, Chang Bum L, Stefanovich G, Chang Jung K, Youngsoo P (2009) Stackable all-oxide-based nonvolatile memory with Al_2O_3 antifuse and p-CuO_x/n-$InZnO_x$ diode. IEEE Electron Device Lett 30:550–552. doi:10.1109/LED.2009.2016582
290. Sato Y, Tsunoda K, Kinoshita K, Noshiro H, Aoki M, Sugiyama Y (2008) Sub-100-μA reset current of nickel oxide resistive memory through control of filamentary conductance by current limit of MOSFET. IEEE Trans Electron Devices 55:1185–1191. doi:10.1109/TED.2008.919385
291. Wei Z, Kanzawa Y, Arita K, Katoh Y, Kawai K, Muraoka S, Mitani S, Fujii S, Katayama K, Iijima M, Mikawa T, Ninomiya T, Miyanaga R, Kawashima Y, Tsuji K, Himeno A, Okada T, Azuma R, Shimakawa K, Sugaya H, Takagi T, Yasuhara R, Horiba K, Kumigashira H, Oshima M (2008) Highly reliable TaO_x ReRAM and direct evidence of redox reaction mechanism. IEEE Int Electron Devices Meet 2008:1–4. doi:10.1109/IEDM.2008.4796676
292. Jeong DS, Schroeder H, Waser R (2007) Coexistence of bipolar and unipolar resistive switching behaviors in a Pt / TiO[sub 2] / Pt stack. Electrochem Solid-State Lett 10:G51. doi:10.1149/1.2742989
293. Kim S, Byun I, Hwang I, Kim J, Choi J, Park BH, Seo S, Lee MJ, Seo DH, Suh DS, Joung YS, Yoo IK (2005) Giant and stable conductivity switching behaviors in ZrO2 films deposited by pulsed laser depositions. Japanese J Appl Physics, Part 2 Lett 44:2–5. doi:10.1143/JJAP.44.L345
294. Cao X, Li X, Gao X, Yu W, Liu X, Zhang Y, Chen L, Cheng X. Forming-free colossal resistive switching effect in rare-earth-oxide Gd2 O3 films for memristor applications. J Appl Phys. doi: 10.1063/1.3236573
295. Murugan AV, Navale SC, Ravi V (2006) Synthesis of nanocrystalline La 2 O 3 powder at 100 ° C 60:848–849. doi: 10.1016/j.matlet.2005.10.030
296. Yu D, Liu LF, Chen B, Zhang FF, Gao B, Fu YH, Liu XY, Kang JF, Zhang X (2011) Multilevel resistive switching characteristics in Ag/SiO_2/Pt RRAM devices. IEEE Int Conf Electron Devices Solid-State Circuits 2011:1–2. doi:10.1109/EDSSC.2011.6117721
297. Chung YL, Cheng WH, Jeng JS, Chen WC, Jhan SA, Chen JS (2014) Joint contributions of Ag ions and oxygen vacancies to conducting filament evolution of Ag/TaOx/Pt memory device. J Appl Phys 116:2012–2017. doi:10.1063/1.4899319
298. Lin C, Chang Y (2012) Formation and Rupture of Ag Conductive Bridge in ZrO 2 -Based Resistive Switching Memory Delivered by Ingenta to 12:2437–2441. doi: 10.1166/jnn.2012.5768
299. Tsunoda K, Fukuzumi Y, Jameson JR, Wang Z, Griffin PB, Nishi Y (2007) Bipolar resistive switching in polycrystalline TiO2 films. Appl Phys Lett 90:2005–2008. doi:10.1063/1.2712777

Submit your manuscript to a SpringerOpen journal and benefit from:

- ► Convenient online submission
- ► Rigorous peer review
- ► Immediate publication on acceptance
- ► Open access: articles freely available online
- ► High visibility within the field
- ► Retaining the copyright to your article

Submit your next manuscript at ► springeropen.com